Key Controls on the Hydraulic Properties of Fault Rocks in Carbonates

E. A. H. Michie [1, 2]*, A. P. Cooke[3], I. Kaminskaite[3, 4], J. C. Stead[3], G. E. Plenderleith[3, 5], S. D. Tobiss[3], Q. J. Fisher[3, 4], G. Yielding[1], B. Freeman[1]

[1] Badleys Ltd, North Beck House, North Beck Lane, Hundleby, Spilsby, Lincolnshire, PE23 5NB, UK

[2] Current address: Department of Geosciences, University of Oslo, Sem Sælands Vei 1, Oslo 0371, Norway

[3] School of Earth and Environment, University of Leeds, Leeds, LS2 9JT, UK

[4] Petriva Ltd. University of Leeds, Leeds, LS2 9JT, UK

[5] Current address: British Geological Survey, The Lyell Centre, Edinburgh, EH14 4AP, UK

***Corresponding author:** e.m.haines@geo.uio.no

Keywords: fault rock; carbonates; microstructures; fault seal; porosity; permeability

Abstract

A significant knowledge gap exists when analysing and predicting the hydraulic behaviour of faults within carbonate reservoirs. To improve this, a large database of carbonate fault rock properties has been collected from 42 exposed faults, from 7 countries. Faults analysed cut a range of lithofacies, tectonic histories, burial depths and displacements. Porosity and permeability measurements from *c.*400 samples have been made, with the goal of identifying key controls on the flow properties of fault rocks in carbonates. Intrinsic and extrinsic factors have been examined, such as host lithofacies, juxtaposition, host porosity and permeability, tectonic regime, displacement, maximum burial depth as well as the depth at the time of faulting. The results indicate which factors may have the most significant influence on fault rock permeability, improving our ability to predict the sealing or baffle behaviour of faults in carbonate reservoirs. Intrinsic factors, such as host porosity, permeability and texture, appear to play the most important role in fault rock development. Extrinsic factors, such as displacement and kinematics, have shown lesser or, in some instances, a negligible control on fault rock development. This conclusion is, however, subject to two research limitations: lack of sufficient data from similar lithofacies at different displacements, and a low number of samples from thrust regimes.

Faults have been shown to exert significant control on fluid flow within the subsurface. Research determining the conditions in which faults act as conduits, barriers or partial barriers to flow in siliciclastic reservoirs has been widely documented (e.g. Knipe 1992; Caine et al., 1996; Yielding et al., 1997; Fisher and Knipe 1998; 2001; Bretan et al., 2003; Flodin et al., 2005; Yielding 2015). It is considered that faults within a sand-shale sequence containing a high proportion of shale have a high potential for clay smear or gouge to be generated, lowering the permeability to create a baffle or seal (Yielding et al., 1997; 2010; Fisher and Knipe 1998). On the other hand, faults in clay-poor sandstones may have their permeability lowered by cataclasis and post-faulting quartz cementation (Fisher and Knipe 1998). This understanding can help to reduce uncertainty when estimating the hydraulic properties of fault zones in the subsurface. However, limited research has been undertaken on the impact of faults on fluid flow in carbonate reservoirs, despite their importance in global hydrocarbon reserves; around 60% of global oil reserves and 40% of global gas reserves are stored in carbonates (Al-Anzi et al., 2003). Faulted carbonates have been documented as having a range of sealing potentials, from barriers to conduits, or dual conduit-seal characters (Billi et al., 2003; Celico et al., 2006; Agosta 2008; Michie et al., 2018). Despite this fact, there is currently no simple measure of seal potential (analogous to the Shale Gouge Ratio) for faulted carbonates that lack shaley interbeds.

Fault zone architecture, evolution and fracture patterns in carbonates have recently received significant attention (e.g. Billi et al., 2003; Micarelli et al., 2006; Ferrill and Morris 2008; Bastesen and Braathen 2010; Molli et al., 2010; Ferrill et al., 2011; Michie et al., 2014; Agosta et al., 2015; Bussolotto et al., 2015; Fondriest et al., 2015; Rustichelli et al., 2016). Also, research has recently been conducted on the deformation mechanisms and microstructures of carbonate fault rocks (Bastesen et al., 2009; Rath et al., 2011; Michie 2015; Schröckenfuchs et al., 2015; Cooke et al., 2018; Ferraro et al., 2018; Kaminskaite et al., 2019). However, there is surprisingly little data on the porosity and permeability of carbonate fault rocks (e.g. Agosta et al., 2007; Bastesen et al., 2009; Haines et al., 2016; Michie and Haines 2016; Tondi et al., 2016; Cooke et al., 2020; Kaminskaite et al., 2020). By the time of this publication, authors were aware of only one publicly available documented study where petrophysical data has been used in a predictive sense for calculation of carbonate fault rock permeability and transmissibility multipliers in a cellular model (Michie et al., 2018).

A variety of deformation mechanisms have been documented in faulted carbonates. It has been shown that deformation bands cutting high porosity host rocks, form from a range of mechanisms, including grain crushing, rotation and translation, cementation, pressure solution, peloid disintegration and smearing (Tondi et al., 2006a; Rath et al., 2011; Cilona et al., 2012; Antonellini et al., 2014; Rotevatn et al., 2016; Kaminskaite et al., 2019). The mechanisms vary according to host texture and composition as well as the stress conditions at the time of faulting (Kaminskaite et al., 2019). Despite the variation in mechanisms, deformation bands generally show a decrease in porosity and permeability from the host, varying as a function of evolution (Rath et al., 2011; Antonellini et al., 2014; Tondi et al., 2016; Kaminskaite et al., 2019). Deformation mechanisms and microstructures of fault rocks in highly porous carbonates, with throws larger than deformation bands, are less well documented (e.g. Michie 2015; Cooke et al., 2018). In these examples, the deformation mechanisms vary according to lithofacies, and range from grain-scale cataclasis to brecciation, recrystallisation or purely cementation with no grain crushing, creating a variety of fault rock fabrics. Consequently, the petrophysical properties of these fault rocks vary with lithofacies and have been shown to also vary with how the lithofacies are juxtaposed at different displacements (Michie and Haines 2016).

Fault rocks in low porosity carbonates are more widely documented, showing brittle deformation mechanisms such as fracturing, veining and brecciation (Agosta and Kirschner 2003; Billi et al., 2003; Micarelli et al., 2006; Bussolotto et al., 2007; Molli et al., 2011; Bussolotto et al., 2015; Schröckenfuchs et al., 2015; Bauer et al., 2016; Ferraro et al., 2018; Ferraro et al., 2019; Ferraro et al., 2020; Kaminskaite et al., 2020). The porosity and permeability of faults in low porosity carbonates are shown to gradually increase from the host rock into the fault zone, with a decrease in porosity and permeability in the inner fault core immediately surrounding the principal slip surface (Agosta et al., 2007). However, porosity and permeability values of these fault core samples are often similar to the values of the host.

To assess across-fault flow potential, and consequently, reservoir compartmentalisation, the distribution and petrophysical properties of fault rock within a fault zone must be determined. Accordingly, the research presented here works towards a predictive method to estimate fault rock permeability in carbonate rocks based upon key lithological and fault parameters. The data presented within this paper were collected as part of a consortium project with the ultimate aim of establishing an algorithm to predict fault rock permeability in carbonates. We present microstructural and petrophysical properties from a range of carbonates with varying host textures, porosities and permeabilities, and from varying tectonic settings.

Geological Background

In this paper, we document sampled fault zones from multiple localities in seven different countries, namely Germany, Greece, Italy, Malta, Oman, UAE and UK. Samples from Germany, Italy, Oman, UAE are from lithofacies with low host porosity and permeability. The majority of these samples have been recrystallized, occluding porosity, and have been buried to significant depth, 1-6 km (Figure 1). The kinematics of these fault zones vary from normal faulting (Germany, Italy, Oman and UAE), strike-slip (Italy and UAE) to thrust faulting (Oman and UAE). Samples from Greece, Italy, Malta and UK are from hosts with relatively high host porosity and permeability. The host lithofacies from these localities cover the majority of the Dunham classification (Dunham 1962), including chalk, with the exception of mudstones (Figure 2). These samples have been buried to shallower depths, <1 km. The kinematics of these faults are primarily either low strain deformation bands (all four localities) or normal, oblique and strike-slip faults (Maltese Islands). Fault displacement from all localities ranges from millimetre offset, creating deformation bands, up to 5 km. Details for each locality have been summarised into Table 1.

Germany

The Elbingerode complex, Central Harz Mountains, Germany, consists of Palaeozoic deposits from the Rhenohercynian fold belt as part of deformation from the Eastern extent of the Variscan orogeny (Brink 2011). Extensional tectonics then followed during the Cretaceous. The studied outcrop consists of Devonian reef carbonates, capping three volcanic edifices, creating a localised high-temperature gradient (Fuchs 1987; Weller 1991; Brink 2011). A *c.*100 m displacement normal fault cuts low porosity (*c.*1%), recrystallised packstones (Figure 1A) and has been buried to a maximum depth of *c.*3 km, which is also estimated as the depth at the time of faulting based on geological restoration (Stead 2018).

Greece

Samples were collected from deformation bands in Rhodes that formed due to the collapse of the Aegean Sea during the Arabian-Eurasian plate collision in the Pliocene. Later, sinistral strike-slip faulting occurred due to the increased curvature of the plate boundary (ten Veen and Kleinspehn 2002). Depth at the time of faulting is estimated as 520 m, based on total sea-level fall (Cornée et al., 2006). Deformation bands cut the Cape Arkhangelos calcarenite formation; a high porosity (*c.*43%), bioclastic grainstone containing a high percentage (>50%) of peloids (Figure 2C) (Hanken et al., 1996; Kaminskaite et al., 2019).

Italy

Several localities have been studied in both mainland Italy and Sicily: NW Sicily, SW Italy and Gargano promontory.

NW Sicily

NW Sicily is part of the western edge of the Sicilian-Maghrabian fold-thrust belt, active during the Cenozoic due to collision between the North-African margin and Sardinia-Corsica block, composed of south-verging folds and thrusts. Deformation occurred by E-W trending thrusting in the Early Miocene, followed by extensional faulting in the Late Miocene and strike-slip faulting in the Plio-Pleistocene (Catalano et al., 1985; Giunta et al., 2000). Two very different styles of deformation were examined in NW Sicily: deformation bands in high-porosity (*c.*47%) Upper Pliocene-Lower Pleistocene bioclastic grainstones (Figure 2A; Table 1: NW Sicily (a)) that have been shallowly buried to *c.*50 m (Abate et al., 1997; Kaminskaite et al., 2019), and larger-scale faulting (metres to tens of metres offset) in low-porosity (<2%), recrystallised packstones and dolostones, of Cretaceous and Triassic age, respectively

(Kaminskaite et al., 2020; Figure 1F, Table 1: NW Sicily (b)). Maximum burial depths for the Triassic Pellegrino Quarry dolomite, Triassic Monte Cofano dolomite and Mid-Upper Cretaceous San Vito Lo Capo packstones are 3100 m, 2910 m and 1970 m, respectively. Depth at the time of faulting has been estimated as 2200 m at Monte Cofano, associated with the Miocene thrust event (Tondi et al, 2006b), and 290 m and 200 m at Pellegrino Quarry and San Vito Lo Capo, respectively, associated with the Plio-Pleistocene strike-slip events (Tondi et al, 2006b), based on geological restorations (Stead 2018; Kaminskaite et al., 2020).

SW Italy

Three main localities have been examined in SW Italy: Sala Consilina, Monte Alpi and Villa D'Agri. All localities are found within the axial portion of the Southern Apennines, a NE-propagating compression belt driven by the collision of Eurasian and African plates from the Miocene to Early Pleistocene. These faults cut low-porosity (<10%) Jurassic-Cretaceous Apulian and Apenninic platform limestones and dolomites (Figure 1B), ranging from recrystallised mudstones to grainstones (Corrado et al., 2002; Van Dijk et al., 2000; La Bruna et al., 2017; La Bruna et al., 2018). The faults are normal at Villa D'Agri and strike-slip at Sala Consilina, and both normal and strike-slip at Monte Alpi, with displacements varying from 50 m up to 5 km, and depths of burial of *c.*1 km for Sala Consilina, *c.*1500 m for Villa D'Agri samples, and *c.*6 km at Monte Alpi (Corrado et al., 2002; La Bruna et al., 2017; La Bruna et al., 2018). Depth at the time of faulting is estimated as 390 m, 920 m and 3780 m for Sala Consilina, Villa D'Agri and Monte Alpi, respectively (Stead, 2018).

Gargano promontory

Deformation bands have been studied at the Gargano promontory, which has been subjected to two kinematic events related to the Mattinata Fault System: a left-lateral event in the Late Miocene – Early Pliocene, followed by a right-lateral motion in the Late Pliocene (Chilovi et al., 2000). The deformation bands cut the Gravina calcarenite succession, which is a shallowly buried (*c.*350-400 m), high-porosity (*c.*38%) bioclastic grainstone (Casolari et al., 2000; Tropeano and Sabato 2000; Kaminskaite et al., 2019).

Maltese Islands

Faults on Malta and Gozo are generally oriented ENE-WSW and NW-SE, and formed during the Pliocene-Quaternary as part of the transtensional system in the foreland of the Sicilian Apennine-Maghrabian fold-thrust belt (Pedley et al., 1976; Dart et al., 1993). The faults cut a range of formations with lithofacies varying from wackestones (25-36% porosity) (Figure 2E) to packstones (20-35%) (Figure 2D) and algal packstones (10-15% porosity) (Figure 2F), which have been shallowly buried to depths of 300 m to 1000 m, which are also estimated as the depths at the time of faulting (Dart et al., 1993; Peacock 2001; Kim et al., 2003; Bonson et al., 2007; Michie and Haines 2016; Cooke et al., 2018).

Oman

Samples have been collected from three main localities: Wadi Dayqah Dam, Wadi Nakhr and Wadi Mistal. These localities are found across the Oman Mountains, which were formed as part of the Alpine-Himalayan chain from a northeast-directed subduction of the Arabian Plate below the Eurasian Plate (Searle 1985; Al Kindy and Richard 2014). Large faults cut low porosity (<6%) recrystallised Cretaceous carbonates, ranging from mudstone to grainstone lithofacies (Figures 1C and D) that have been buried to several kilometres, generating high temperatures of up to around 250°C (Droste and Van Steenwinkel 2004; Holland et al., 2009; Vandeginste et al., 2013; Richard et al., 2014; Grobe et al., 2016). Fault kinematics vary from normal to thrust faulting.

UAE

The United Arab Emirates is located within the interior platform of the Arabian shelf, bounded on the NW by the Qatar-South Fars Arch, and on the east and NE by the foreland basin, and adjacent foreland fold-thrust belt of Oman (Alsharhan 1989). The studied faults occurred both offshore UAE and also in the Oman Mountains in East UAE. The faults outcropping in the Oman Mountains cut carbonates from the Permian to Cretaceous, which have been recrystallised, creating low porosities (<7%) (Figures 1E). Maximum burial depth and depth at the time of faulting are the same, and range between 1.5 and 4 km (Stead 2018). Offshore, faults cut wackestones, packstones and grainstones with high porosities (>20%). Maximum burial depth is *c.*2-3.5 km, with depth at time of faulting unknown. Faulting varies from small-scale deformation bands to faults with tens of metres throw, with varying kinematics; from normal to strike-slip and thrust faults.

UK

Deformation bands have been studied from the Isle of Thanet, SE England, consisting of a monocline of Upper Cretaceous Chalk, which was exposed to deformation from E-W extension, then later NE-SW extension in the late Cretaceous and Tertiary inversion (Bergerate and Vandycke 1994; Ameen 1995; Vandycke 2002). The chalk has a high porosity, from 39 to 45%, and is composed predominantly of a micritic matrix with a minor proportion (*c.*15%) of bioclasts such as foraminifera (Figure 2B). It has been shallowly buried to a maximum depth of *c.*300-500 m, which is also taken as the depth at time of faulting (Kennedy and Garrison 1975; Welch et al., 2015).

Method

Outcrop and laboratory techniques have been undertaken on the studied faulted carbonates. Microstructural analysis, used to identify the deformation mechanisms that form specific fault rock fabrics, has been combined with measured porosity and permeability values to define relationships of fault rock development, based on both instrinsic and extrinsic factors. Intrinsic factors included lithofacies (texture), lithofacies juxtaposition, host porosity and host permeability. The extrinsic factors considered were kinematics, fault displacement and depth at the time of faulting. The identified relationships are used to analyse the across-fault fluid flow potential of faults in distinct geological settings, improving our ability to predict the flow properties of carbonate fault zones.

Sample collection

Over 600 oriented samples of both fault rocks and their respective host lithofacies have been collected using a hammer and chisel from outcrops over several field campaigns. Samples from subsurface cores from industry sponsors have also been gathered. These two sets of samples (from outcrops and cores) were used to analyse fault rock development and petrophysical properties.

Microstructural analysis

Oriented fault rock samples were used for optical thin-section and scanning electron microscope-backscatter electron microscopy (SEM-BSE) analysis of deformation microstructures to infer the mechanisms involved in producing each microstructure.

Fault rock samples were oriented parallel and perpendicular to fault dip. Samples were impregnated with low viscosity resin containing blue epoxy dye, under vacuum on low permeability samples, to make pore spaces more apparent when viewed using optical microscopy. Thin sections of the host-rock, oriented perpendicular to bedding, were used to examine the representative composition and textures of different lithofacies, as well as their heterogeneity. Specifically, the types of pores and grains were examined. The associated fault rock types can then be related to specific host textures.

Classification of whether fault rocks behave in a brittle or ductile manner are based on grain-scale processes by deformation microstructures observed, rather than how they would deform according to their stress-strain behaviour.

Porosity and permeability measurements

Petrophysical measurements have been made on *c.*400 samples. Core plugs were taken adjacent to the representative thin sections, to accurately capture the porosity and permeability of each varying fault rock and host rock microstructure. These core plugs were cleaned to remove salts using deionised water saturated with carbonate sediment of the same composition as the sample, and then dried at 65°C for between 3 and 7 days.

Porosity

Porosity, ø, was calculated by subtracting the grain volume, V_g, from the bulk volume, V_b using:-

$$\emptyset = \frac{V_b - V_g}{V_b}$$

The grain volume was measured using a Quantachrome Stereopycnometer SPY-3 helium pycnometer, by defining the ratio between load pressure and final pressure, based on Boyle's law double-cell method. The measurements were repeated three times to reduce experimental error, and the arithmetic mean values were taken. The bulk volume was calculated from measurements of the length and diameter of the core plugs using a digital calliper, with a precision of 0.01 mm.

Permeability

Single-phase helium permeability measurements were acquired using a CoreLab 200 PDP pulse-decay permeameter, adapted to perform both steady-state and pulse-decay methods for high (>1 mD) and low (<1 mD) permeability samples, respectively. Samples were loaded into a rubber sleeve within a core holder. Confining pressures equivalent to the mean effective stresses estimated for each locality when at its maximum burial depth were applied. In pulse-decay permeability tests, the pore pressure was increased and allowed to equilibrate, after which a differential pressure was introduced and both the absolute and differential pore pressures were monitored until the pressure re-equilibrated. Permeability was calculated using the methods of Jones (1997). For steady-state tests, constant upstream pressure was applied while the downstream was vented through a flowmeter. The differential pressure across the sample was monitored until it stabilised, where the flow rate, differential pressure and pore pressure were recorded to calculate permeability at a certain pore pressure, according to Darcy's Law.

The permeability was corrected for gas slippage at low pressures using the Klinkenberg method (Klinkenberg 1941). A linear regression of the apparent permeability with the reciprocal of the mean pore pressure, 1/P, was plotted using several mean pore pressures (≥ 4 data points). The intercept on the permeability axis gives the Klinkenberg corrected permeability.

Controls on Fault Rock Development: Results

The porosity and permeability of carbonate fault rocks show significant variation (Figure 3), with porosity varying over 46% and permeability varying over 10 orders magnitude, from a nanodarcy to over a Darcy. The petrophysical properties of fault rocks can also vary along-strike and down-dip on a single fault surface. Trends to fault rock porosity and permeability are observed based on factors which control deformation style, influencing the fault rock development. The inferred mechanisms from observed microstructures creating the fault rocks range from elasto-frictional to crystal-plastic deformation, and depend on factors such as burial depth at the time of faulting and lithofacies.

Lithofacies

Deformation style has been observed to vary across the range of Dunham textures (*cf.* Dunham 1962). Lithofacies with high micritic content, such as mudstones and wackestones, which are characterised by a matrix-supported texture and can have a high porosity (>10%), have been shown to deform by disperse fractures. Increased fracturing leading to brecciation can evolve further to create cataclasite fault rocks, similar to that described by Billi et al. (2003) (Figure 4). This deformation style is observed in all matrix–supported lithofacies, regardless of host porosity (Figure 4). Grain-supported lithofacies with high algal content, such as algal-rich packstones, floatstones, rudstones or boundstones, and lithofacies that have been heavily recrystallised creating a low porosity rock (<10%), also behave similarly, deforming by disperse fracturing/brecciation evolving into cataclasis (Figure 4).

On the other hand, lithofacies with minimal micritic content, i.e. those that are grain-supported, with low algal content, and high porosity (>10%), such as grainstones and bioclastic packstones, are shown to deform by localised mechanisms breaking down individual grains, progressing to grain-scale cataclasis.

It is important to note however, that the documented observations recorded above are grain-scale brittle microstructures. At higher pressures and temperatures, grain-scale ductile mechanisms are observed to dominate (discussed in the Burial Depth section below).

How each lithofacies deforms dictates which fault rocks are produced, and hence also influences the hydraulic behaviour, as each fault rock type has varying porosity and permeability. Generally, a decrease in the porosity and permeability of the fault rocks is observed with increasing micritic content or crystallinity (Figure 5A). However, it is important to also compare the fault rock permeability to that of the host, rather than simply examining the current poroperm of the fault rocks, as it is the difference between the host and fault rock permeabilities that controls whether the fault acts as a baffle or conduit. Plotting the permeability contrast between the host and fault rock samples, we can see that some lithofacies show an increase in the permeability of the fault rock ***relative*** to the host rock values, while other lithofacies show a decrease in ***relative*** permeability (Figure 5B). Those lithofacies that have a tendency to deform by grain-scale cataclasis show the largest decrease in permeability with respect to the host values, namely grainstones and packstones. As mentioned previously, lithofacies such as algal-rich packstones, wackestones and crystalline carbonates, have the tendency to deform by through-going fracturing, evolving to brecciation and then disperse cataclasis. While these deformation styles often leads to an increase in ***relative*** permeability for crystalline samples, a decrease in ***relative*** permeability is recorded for the majority of wackestone and algal packstone samples, albeit with a lower permeability contrast than those samples that deform by grain-scale cataclasis (Figure 5B). Moreover, although the studied fault rocks in crystalline lithofacies generally show an increase in ***relative*** permeability from the host values, their respective host samples have very low ***absolute*** matrix permeabilities (around 0.000001-0.01 mD), hence their ***absolute*** value remains low. Chalk samples do not show a significant permeability change (Figure 5B). This lithofacies deforms by breaking down large, isolated foraminifera that act to decrease the porosity, whilst allowing the permeability to remain the same (Kaminskaite et al., 2019).

Lithofacies Juxtaposition

Not only does lithofacies have significant control on fault rock development, but how the lithofacies are juxtaposed is also a crucial factor that requires further examination. An increased fault core heterogeneity has been observed when juxtaposition of different lithofacies occurs. Specifically, several different fault rock types, with a variety of deformation and/or diagenetic microstructures, are observed along fault-strike at juxtapositions of different lithofacies. This leads to an increase in the range of permeability values. Conversely, a relatively homogeneous fault core, with similar microstructures and permeability values, is observed along fault-strike at either self-juxtapositions or juxtaposition of similar lithofacies (Figure 6). However, it is important to note that despite the initial textural variation that can occur in crystalline host rocks with low porosity/permeability, the overall mechanical and petrophysical properties of these recrystallised lithofacies are very similar. Hence, at the juxtaposition of two recrystallised lithofacies with different initial textures, similar microstructures along fault-strike are observed.

Mineralogy

The influence of mineralogy on fault rock porosity and permeability has been examined, dividing the data by calcite versus dolomite host rock and their respective fault rocks (Figure 7A), as well as the current mineralogy of the fault rock (Figure 7B). In order to compare only similar materials, we have plotted faults that cut low porosity, low permeability calcite host rocks, and omitted those with higher porosities and permeabilities, as only faults cutting low porosity and low permeability dolomitic host rocks have been sampled. We can see that there is significant overlap between fault rocks that cut calcite and dolomite, and both examples can show an increase in both porosity and permeability from the host values (Figure 7A). The only notable difference between fault rocks that cut calcite or dolomite host rocks is faults in dolomite show a slightly higher average fault rock permeability (0.04 mD geometric mean) when compared to those that cut calcitic host rocks (0.0075 mD geometric mean). However, this could simply be a product of the low number of example faults in dolomite, and hence the lack of ability to compare samples with constant external factors, such as displacement and depth of burial. When comparing fault rocks with current differing mineralogy, we can see significant overlap in the porosity and permeability values, with no discernible relationships (Figure 7B). However, it is shown that some of the fault rocks with mixed calcite and dolomite mineralogy have higher porosity values, regardless of whether the original mineralogy was calcite or dolomite (Figure 7).

Host Porosity and Permeability

Dividing the data into faults that cut host rocks with an average low porosity, <10% (Figure 8A), and average high porosity, >10% (Figure 8B), allows us to better visualise the relationships between the host porosity and permeability and the fault rock porosity and permeability. Fault rock samples in low porosity carbonates do not show a decrease in the porosity and permeability. Instead, the porosity and permeability values are often recorded as being higher than their respective host samples (Figure 8C). Conversely, the porosity and permeability values of fault rocks cutting high porosity carbonates generally show a decreased value from the host samples (Figure 8D).

Further to the analysis above, we can also examine how the fault rock permeability, and the permeability contrast between host and fault rock permeability, vary with host porosity (Figure 9A, C, E) and host permeability (Figure 9B, D, F). Although significant scatter is observed when examining individual fault rock permeability points with both host porosity and host permeability (Figure 9A, B), this scatter is reduced when the geometric mean is taken for fault rock permeability per lithofacies, per locality (Figure 9C, D). When the geometric mean values are weighted based on number of raw data points, this acts to strengthen the trend, and hence increases the R^2 value. An ***absolute*** increase in fault rock permeability is shown with increasing host porosity (Figure 9C), however a decrease in the fault rock permeability is observed ***relative*** to the host for the majority of samples with an average host porosity >10%. Samples with an average host porosity <10% mostly show an increase in permeability ***relative*** to the host (Figure 9E). Since host porosity and texture (lithofacies) influences the host permeability, a similar relationship is also observed between host permeability and fault rock permeability (Figure 9B, D, F). An ***absolute*** increase in fault rock permeability occurs with increasing host permeability (Figure 9D), however a decrease in the fault rock permeability ***relative*** to the host occurs for the majority of samples with an average host permeability >0.1 mD (Figure 9F).

Kinematics

There is significant scatter to the porosity and permeability data for fault rocks formed in each tectonic regime, with no patterns to particular kinematics influencing the fault rock permeability in a similar manner. The only exception is that deformation bands generally have higher porosity and permeability than all other, more evolved, fault rocks (Figure 10). Moreover, similar deformation and diagenetic microstructures are observed regardless of kinematics (Figure 10). In this example, two dolomitic recrystallised lithofacies deform similarly in both a large strike-slip fault and a normal fault; this lithofacies shows disperse fracturing, fracture-evolved cataclasis and cementation/veining (Figure 10).

Displacement

Absolute fault rock permeability values show a decrease from the protolith when displacement exceeds 1 m (i.e. fault rock samples larger than deformation bands). However, no discernible relationship to fault rock permeability is observed beyond 1 m displacement (Figure 11A). Below 1 m displacement only deformation bands are observed, which show higher absolute permeability values, associated with the lower strain creating these deformation bands (Figure 11A). Plotting the permeability contrast between the host and fault rock with displacement shows significant scatter, with no relationship observed between the relative permeability of fault rocks and displacement, at displacements over 1 m (Figure 11B). There is, however, a decrease in ***relative*** permeability for almost all deformation bands (shown at 0.01 m displacement), despite their ***absolute*** high permeability values. The observed scatter may be exaggerated by other factors overprinting possible relationships. Hence, we have furthered this analysis by examining how the permeability of similar lithofacies varies with displacement (Figure 11C). In this example, we show fault rock permeability cutting low permeability, recrystallised lithofacies at low (*c.*10 m) and high (*c.*100 m) displacement. We have observed that regardless of displacement, there is no obvious trend showing how the permeability of fault cores may evolve; the median permeability in this example is the same at both low and high displacements (Figure 11C).

Burial Depth

The maximum burial depth and depth when faulting occurred is observed to influence the mechanisms active during creation of fault rocks, and hence also their petrophysical properties. Generally, grain-scale brittle mechanisms such as fracturing, brecciation and cataclasis are predominantly observed at shallower depths (Figure 12A, B). At greater depths, ductile mechanisms are observed to prevail over brittle mechanisms, forming highly recrystallized fault rocks with low permeability (Figure 12C, D, with a fault rock permeability of 0.00022 mD in this example). Mechanisms such as twinning, grain boundary migration and grain bulging are common in the samples from greater depths and temperatures (e.g. Figure

12D). Note that in this context, the terminologies brittle and ductile are not based on mechanical behaviour derived from experimental strain-strain curves, but simply based on observed microstructures.

Average fault rock permeability is observed to decrease with both increasing maximum burial depth (Figure 13A) and depth at the time of faulting (Figure 13B), up to 1-2 km. Beyond 1-2 km, the trend of fault rock permeability decreasing with depth of burial and depth at the time of faulting is shown to flatten off to mean values of around 0.01 mD (Figure 13). The range of permeability is also observed to decrease with increasing depth at the time of faulting (Figure 13B). However, it is important to note that very low fault rock permeability values can occur at both shallow and greater depths of burial and depths at time of faulting, and that the lowest permeability values are recorded at maximum burial depths of between 1-2 km (Figure 13A) and <1 km depth at time of faulting (Figure 13B). Note that the R^2 value is higher for trends with maximum burial depths when compared to depth at the time of faulting.

Discussion

Research into deformation surrounding faults in carbonates has received significant attention in the last couple of decades (e.g. Tondi et al., 2006a; Ferrill and Morris 2008; Agosta et al., 2010; Bastesen and Braathen 2010; Michie et al., 2014; Cooke et al., 2018; Kaminskaite et al., 2020). However, the ability to predict the hydraulic behaviour of faults in carbonates was largely unknown, with very few publications documenting our advances in carbonate fault seal analysis (e.g. Solum and Huisman 2017; Michie et al., 2018). Here, we have attempted to expand our understanding of the main controls on fault rock development and their petrophysical properties to improve our ability to predict their hydraulic behaviour in the subsurface.

Intrinsic Factors

Our observations within this study, based on a wide range of data, indicate that intrinsic factors are the primary control on fault rock development. Host lithofacies plays a crucial role in deformation style, creating specific fault rock types within different lithofacies. Each fault rock type will have differing petrophysical properties. Hence, host lithofacies will influence the permeability of the fault rock. Moreover, how different lithofacies are juxtaposed, and what the overall succession is composed of, seems to also dictate the hydraulic behaviour of the fault. However, further work is required to confirm this juxtaposition hypothesis due to a relatively limited number of examples showing juxtaposition of different lithofacies in our database.

Lithofacies with a high micritic content has shown to deform in a similar manner to those that have been recrystallised. This is due to the relatively homogeneous mechanical properties within these rocks, creating low/no mechanical discontinuities. Mechanical contrasts are necessary for grain-scale fragmentation (Kranz 1983; Groshong 1988). Hence, fractures can easily propagate throughout these matrix-supported lithofacies and create a variety of breccias and cataclasites, depending on the evolution stage (Figure 4). Further, algal-supported lithofacies also deform by fracturing and brecciation, as algae have been observed to not cataclase; they protect the bioclast grain-grain contacts, preventing grain-scale cataclasis. Conversely, grain-supported lithofacies commonly experience grain-scale cataclasis due to the high mechanical discontinuities throughout the rock, e.g. between bioclastic grains and pores (*cf.* Kranz 1983; Groshong 1988). The clast-confined fractures nucleate at grain boundaries, creating impingement microcracks, which break down individual bioclasts, and can evolve to cataclase the rock (Figure 4). Moreover, diagenesis, specifically aggrading neomorphism, has been observed in grain-supported lithofacies immediately surrounding slip surfaces, often with no other deformation microstructures such as fracturing or fragmentation observed (Michie 2015). The increased cementation in grain-supported lithofacies could simply reflect the higher initial permeability.

Similar observations have been documented in carbonate lithofacies by other authors, where different microstructures are observed in carbonates with varying porosity, pore types, textures and clay content (Solum and Huisman 2016; Delle Piane et al., 2017, and references therein). For example, grain-scale cataclasites tend to be observed in high porosity carbonates due to cementation and grain breakdown, which act to reduce the porosity and alter the pore types, and hence decrease the permeability (e.g. Tondi 2007; Rath et al., 2011; Tondi et al., 2016; Zambrano et al., 2017; Zambrano et al., 2018; Kaminskaite et al., 2019). Whereas, through-going fracturing is prevalent in low porosity carbonates, which can evolve to create a variety of breccia types and subsequently lead to cataclasite generation due to the resulting lithons having an aspect ratio that allows for lithon rotation and cataclastic flow to commence (e.g. Billi et al., 2003; Cilona et al., 2019). Further complexities due to textural variations and different pore types have also been shown to influence the deformation styles during faulting in carbonates (Michie 2015; Haines et al., 2016).

Since primary texture influences host porosity and permeability, a relationship is also observed between host porosity/permeability and fault rock permeability due to contrasting deformation style; we have observed that fault rock permeability decreases ***relative*** to the host with increasing host permeability and porosity. The host porosity and permeability influence how the rock deforms; rocks with high initial porosity, such as the grain-supported lithofacies, are observed to deform at the grain-scale, resulting in cataclasis or cementation, occluding pore spaces and decreasing the fault rock permeability ***relative*** to the host. Conversely, a rock with low initial porosity, such as crystalline rocks, has shown to fracture and brecciate, increasing the permeability ***relative*** to the host. This conforms to previously published relationships, describing strain that usually reduces the porosity and permeability in high porosity materials, but increases the porosity and permeability in low porosity materials (Groshong 1988). This has been observed and documented previously in both siliciclastic (e.g. Shipton and Cowie 2003) and carbonate rocks (Cooke et al., 2020), showing the control of porosity on deformation style. Moreover, it is easier to reduce the permeability of a high permeability rock than one with an initial low permeability.

The contrast between host and fault rock permeability defined in this study can be used to qualify those scenarios where faults may act as seals, baffles or conduits. We have observed that host rocks with high initial porosity and permeability will generate the largest contrast with the fault rock, creating fault rocks with relatively low porosity and permeability. Contrastingly, hosts with low initial porosity and permeability (e.g. recrystallised rock) have been shown to create fault rocks with increased permeability from the host, thus potentially acting as conduits. However, it is important to note that to be a valid reservoir, the rocks with low porosity and permeability values will need to be fractured, which will increase the bulk host permeability. It is likely that the matrix texture and petrophysical properties will remain the dominant control on deformation style in these fractured examples. Therefore, despite the increase in fault rock permeability ***relative*** to their host, the ***absolute*** permeability value remains low in these examples, hence the fault rock could form a baffle or seal due to the potential high contrast between the fractured reservoir permeability and fault rock permeability. These relationships can be used as a starting point to generate algorithm(s) for fault seal analysis in faulted carbonates (Figure 9).

We have observed that juxtaposing different lithofacies will lead to a variety of deformation and/or diagenetic mechanisms to occur, due to the observed and previously discussed differences in deformation style between varying lithofacies. This in turn will increase the heterogeneity of the fault core. Since different microstructures have different poroperm values, the greater variety of fault rock types is likely to increase the range of fault rock porosity and permeability within a fault core. Conversely, juxtaposition of similar lithofacies, with either similar textures or mechanical and petrophysical properties, will lower the range of mechanisms active. This will form a relatively homogeneous fault core, composed of similar fault rock types, all with similar porosity and permeability values, reducing the range of porosity and permeability along the fault core. Very few papers have previously documented this result, and those that do are from within the same research group (e.g. Michie and Haines 2016: Michie et al., 2018). However, this is an crucial factor for fault core development and requires further research. Although the increase in range of porosity and permeability at juxtapositions of different lithofacies due to a heterogeneous carbonate sequence may mean that the chances to reduce fluid flow may be decreased, the spatial variability of fault rocks will be increased. This spatial heterogeneity may correspond to a greater tortuosity and hence may increase the potential for the fault to baffle flow. However, this is likely to be dicated by the permeability values of each fault rock, and the range between each fault rock type. Further, it is also important to consider which lithofacies have previously slid past another. Juxtaposing similar lithofacies may lead to the assumption of a homogeneous, low permeability fault core. However, if different lithofacies have previously slid past this location along the fault, it will likely introduce variations to the fault rock formed, and hence may also vary the petrophysical properties. A heterogeneous sequence, with significant variation in lithofacies and properties, is likely to create a heterogeneous fault core with a variety of different fault rock types and porosity and permeability values. Further research, however, is required to confirm such hypothesis, as we have no examples of this scenario within our current database.

The influence of mineralogy on fault rock development has also been assessed. Although mineralogy does not show any strong relationships with fault rock porosity and permeability (Figure 7), it is likely to influence deformation style, not only because mineralogy influences the porosity-depth trend (e.g. Schmoker and Halley 1982; Brown 1997), but also because it has shown to create different mechanical properties (Hugman and Friedman 1979). This in turn will influence the deformation style, and hence also the petrophysical properties (e.g. Bauer et al., 2016; Ferraro et al., 2019; Cilona et al., 2019; Ferraro et al., 2020; Kaminskaite et al., 2020). Dolomite has been recorded as acting in an increased brittle manner when compared to calcite, leading to intensely fractured, pulverised rock at a faster rater than that in limestones, which in turn creates a wide fault zone composed of anastomosing, multiple-stranded cataclasite fault rock (Schröckenfuchs et al., 2015; Fondriest et al., 2015; Bauer et al., 2016; Cilona et al., 2019; Kaminskaite et al., 2020). Further, we can see that those fault rocks with a mixed mineralogy of calcite and dolomite have slightly increased porosity values (Figure 7B). Since these examples cut both dolomite and calcite host rocks, this could be associated with the increase in porosity that can occur with dolomitiztion for those that cut calcite rocks (Warren 2000, and references therein), but also with fracturing and veining introducing calcite-rich fluids to those that cut dolomite rocks. It should be noted, however, that there are limited examples of faults cutting dolomite host rocks, and hence any definitive conclusions cannot currently be drawn.

Extrinsic Factors

The initial observation of our results would indicate that the tectonic regime does not control fault rock development in carbonates. However, it is important to note that, due to the limited number of samples from thrust faults, we cannot definitively conclude the influence of kinematics on the fault rock development. Moreover, kinematics may not show significant influence on fault rock permeability in our samples because of the primary control exerted by host lithofacies texture and host porosity. Hence, any relationships that may occur between kinematics and fault rock permeability may be overshadowed by the overriding control from lithofacies. It is, therefore, important to enhance our knowledge of how kinematics may influence fault rock permeability by gathering more examples of the same/similar lithofacies that have been subjected to different tectonics.

Displacement has been shown to exert significant control on fault rock thickness, where relationships between displacement and thickness have been defined (e.g. Evans 1990; Childs et al., 1996; Sperrevik et al., 2002; Shipton et al., 2006; Wibberley et al., 2008; Braathen et al., 2009; Childs et al., 2009; Bastesen and Braathen 2010; Torabi and Berg 2011; Torabi et al., 2019). Hence, fault rock thickness can be predicted from fault displacement. Similarly, displacement has also been shown to influence fault rock continuity (e.g. Færseth 2006; Cooke et al., 2018), which is crucial when considering whether fluids have the ability to flow across the fault. Both the fault rock thickness and continuity are important parameters for calculating the bulk fault core permeability, and hence are important when predicting and calculating transmissibility multipliers for use in reservoir simulation. Further, fault rock continuity is vital for static fault seal analysis, where areas of zero fault rock thickness will have a massive influence on column height held back by the fault. With that being said, little to no research has been done to identify the control that displacement has on the porosity and permeability of carbonate fault rocks, despite the importance for predicting fault seal in carbonates. In this study, our data shows that displacement has no significant control on the fault rock permeability for fault rock samples created when displacement exceeds 1 m. However, for deformation bands created at displacements of less than 1 m, the relative permeability is decreased from the host rock such that these fault rocks may reduce or impede across-fault fluid flow. The analysis of samples associated to fault displacements over 1 metre (i.e. those with higher strain than deformation bands) has shown that the displacement at which the fault rocks are formed does not appear to influence the microstructures and hence also the fault rock permeability, with mechanisms dependent on host properties rather than strain. Low permeability fault rocks are able to form at low displacements, as well as at higher displacements. A similar finding has also been recorded by Michie and Haines (2016), where similar lithofacies show comparable microstructures and permeability values at both low and high displacements. However, despite our observations and interpretations using our current database, further analysis is required to definitively conclude the impact of displacement on petrophysical properties, due to the low number of examples of similar lithofacies at different displacements. Moreover, any diagenetic overprinting may mask any relationship.

It is well known that the depth at the time of faulting and the maximum burial depth influences the sealing potential of siliciclastic faults, due to increased temperatures and stresses (e.g. Fisher and Knipe 1998; Sperrevik et al., 2002; Yielding et al., 2010). However, little has previously been documented regarding how the fault rock permeability may vary with depth in faulted carbonates. The trend of decreasing permeability, and decreasing range of permeability, with increasing maximum burial depth and depth at the time of faulting may suggest that ductile deformation mechanisms are dominant at greater depths, occluding pore spaces and reducing the permeability and its range. Conversely, the range of fault rock types produced by a variety of brittle mechanisms at shallower depths increases the permeability and its spread, particularly because both low and high porosity host rocks can deform at low burial depths, whereas the rocks deforming at greater burial depths within our database are predominantly from low porosity hosts. This hypothesis is confirmed by examination of the microstructures observed at different burial depths. Brittle microstructures, such as brecciation and cataclasis, are observed to prevail at shallower levels, <1-2 km. We have observed ductile deformation microstructures at depths over 1-2 km, creating recrystallised textures, with little to no porosity and permeability. Other studies have also observed ductile microstructures in carbonate fault rocks at relatively shallow depths of burial and/or low temperatures. For example, plastic deformation has been documented at *c.*1 km (Michie 2015) and 4 km (Bauer et al., 2018) maximum burial depths. Further, it has been well documented that calcite can deform at room temperature by processes such as mechanical twinning, or r-, f- dislocation glide (Turner et al., 1954; Griggs et al., 1960; De Bresser and Spiers 1997). Hence it is predictable that carbonate fault rocks can be formed by ductile processes at shallower burial depths than siliciclastic rocks, which can aid predictions of fault rock permeability. It should be noted that the higher R^2 value for fault rock permeability trend with maximum burial depth, compared to the depth at the time of faulting, may be due to an overriding relationship between porosity and depth (e.g. Schmoker and Halley 1982).

Analysing Key Controls on Fault Rock Development

Analysis using single and multiple regression of the controlling factors showing the greatest influence on fault rock development (i.e. host porosity, host permeability and depth at the time of faulting) has been performed to identify the combination of input parameters that has the primary influence on fault rock permeability for our samples. Table 2 highlights which controlling factors, and combination of controlling factors, have the more significant influence on fault rock development. Surprisingly, it appears that host porosity alone has the greatest influence on fault rock permeability. Moreover, including other factors not only adds no further influence but, in fact, decreases the significance. Hence, trends between host porosity and fault rock permeability could be the most useful input as algorithm(s) for predicting fault hydraulic behaviour in carbonates (i.e. Figure 9A, C, E).

Summary

We have analysed many tens of faults within carbonates from a range of lithofacies, tectonic regimes, burial depths and displacements with the goal of finding trends to fault rock development, in order to generate an algorithm for industry use. Around 400 samples have been collected and analysed, with porosity and permeability measurements made. Intrinsic and extrinsic factors have been analysed to assess their control on fault rock permeabilities. We have observed that intrinsic factors are the dominant control on fault rock development in carbonate faults, with host lithofacies texture and host porosity appearing to be the primary control. Host porosity and texture controls deformation style, fault rock type and hence fault rock permeability. Depth at the time of faulting can also somewhat control deformation style, which in turn influences fault rock permeability. However, for displacements over 1 m (i.e. larger than deformation bands), there is no obvious displacement control on fault rock permeability. Further, kinematics do not show any control on fault rock permeability within our dataset. This may indicate that the fault rocks formed are controlled primarily by other factors, regardless of how and to what extent the rock has moved. Collectively, the results can be used to aid prediction of fault seal behaviour in carbonate sequences, particularly using relationships defined between host porosity and fault rock permeability. Further sampling and analysis are required to confirm and enhance these trends.

Acknowledgements

We thank ADNOC, ENI, OMV, Petrobras and Wintershall Dea for project funding and discussions throughout phase one of the Carbonate Fault Rock project. Partial project funding was also provided by NERC. Peter Bretan, Andrew Foster and Dave McCarthy are warmly acknowledged for discussions and comments to improve the manuscript. The authors would like to thank reviewers John Solumn and Melissa Kiewiet and editor Dave Dewhurst for their thorough and constructive reviews that significantly improved the quality of this manuscript.

References

Abate, B., Incandela, A. and Renda, P., 1997. Carta Geologica delle Isole di Favignana e Levanzo. *Dip. Di Geologia e Geodesia dell'Università degli Studi di Palermo, CoNISMa*.

Agosta, F. and Kirschner, D.L., 2003. Fluid conduits in carbonate-hosted seismogenic normal faults of central Italy. *Journal of Geophysical Research: Solid Earth*, *108*(B4).

Agosta, F., Prasad, M. and Aydin, A., 2007. Physical properties of carbonate fault rocks, fucino basin (Central Italy): implications for fault seal in platform carbonates. *Geofluids*, *7*(1), 19-32.

Agosta, F., 2008. Fluid flow properties of basin-bounding normal faults in platform carbonates, Fucino Basin, central Italy. *Geological Society, London, Special Publications*, *299*(1), 277-291.

Agosta, F., Alessandroni, M., Antonellini, M., Tondi, E. and Giorgioni, M., 2010. From fractures to flow: A field-based quantitative analysis of an outcropping carbonate reservoir. *Tectonophysics*, *490*(3-4), pp.197-213.

Agosta, F., Wilson, C. and Aydin, A., 2015. The role of mechanical stratigraphy on normal fault growth across a Cretaceous carbonate multi-layer, central Texas (USA). *Italian Journal of Geosciences*, *134*(3), 423-441.

Al-Anzi, E., Al-Mutawa, M., Al-Habib, N., Al-Mumen, A., Nasr-El-Din, H., Alvarado, O., Brady, M., Davies, S., Fredd, C., Fu, D., Lungwitz, B., Chang, F., Huidobro, E., Jemmali, M., Samuel, M. and Sandhu, D., (2003). Positive reactions in carbonate reservoir stimulation. *Oilfield Review, winter, 2004*, 28–45.

Al-Kindi, M.H. and Richard, P.D., 2014. The main structural styles of the hydrocarbon reservoirs in Oman. In: Rollinson, H.R., Searle, M.P., Abbasi, I.A., Al-Lazki, A. and Al Kindi, M.H. (eds) Tectonic Evolution of the Oman Mountains. *Geological Society, London, Special Publications*, *392*(1), 409-445.

Alsharhan, A.S., 1989. Petroleum geology of the United Arab Emirates. *Journal of Petroleum Geology*, *12*(3), 253-288.

Ameen, M.S., 1995. Fracture characterization in the Chalk and the evolution of the Thanet monocline, Kent, southern England. *Geological Society, London, Special Publications*, *92*(1), 149-174.

Antonellini, M., Petracchini, L., Billi, A. and Scrocca, D., 2014. First reported occurrence of deformation bands in a platform limestone, the Jurassic Calcare Massiccio Fm., northern Apennines, Italy. *Tectonophysics*, *628*, 85-104.

Bastesen, E., Braathen, A., Nøttveit, H., Gabrielsen, R.H. and Skar, T., 2009. Extensional fault cores in micritic carbonate–case studies from the Gulf of Corinth, Greece. *Journal of Structural geology*, *31*(4), pp.403-420.

Bastesen, E. and Braathen, A., 2010. Extensional faults in fine grained carbonates–analysis of fault core lithology and thickness–displacement relationships. *Journal of Structural Geology*, *32*(11), 1609-1628.

Bauer, H., Schröckenfuchs, T.C. and Decker, K., 2016. Hydrogeological properties of fault zones in a karstified carbonate aquifer (Northern Calcareous Alps, Austria). *Hydrogeology Journal, 24(5),* pp.1147-1170.

Bauer, H., Rogowitz, A., Grasemann, B. and Decker, K., 2018. Crystal plastic deformation in carbonate fault rocks from a shallow crustal strike-slip fault, Northern Calcareous Alps (Austria). In *EGU General Assembly Conference Abstracts* (Vol. 20, p. 9227).

Bergerat, F.T. and Vandycke, S., 1994. Palaeostress analysis and geodynamical implications of Cretaceous-Tertiary faulting in Kent and the Boulonnais. *Journal of the Geological Society*, *151*(3), 439-448.

Billi, A., Salvini, F. and Storti, F., 2003. The damage zone-fault core transition in carbonate rocks: implications for fault growth, structure and permeability. *Journal of Structural geology*, *25*(11), 1779-1794.

Bonson, C.G., Childs, C., Walsh, J.J., Schöpfer, M.P. and Carboni, V., 2007. Geometric and kinematic controls on the internal structure of a large normal fault in massive limestones: the Maghlaq Fault, Malta. *Journal of Structural Geology*, *29*(2), 336-354.

Braathen, A., Tveranger, J., Fossen, H., Skar, T., Cardozo, N., Semshaug, S.E., Bastesen, E. and Sverdrup, E., 2009. Fault facies and its application to sandstone reservoirs. *AAPG bulletin*, *93*(7), pp.891-917.

Bretan, P., Yielding, G. and Jones, H., 2003. Using calibrated shale gouge ratio to estimate hydrocarbon column heights. *AAPG bulletin*, *87*(3), 397-413.

Brown, A., 1997. Porosity variation in carbonates as a function of depth: Mississippian Madison Group, Williston Basin.

Brink, H.J., 2011. The crustal structure around the Harz Mountains (Germany): review and analysis [Die Struktur der Kruste von Harz und Umgebung: Übersicht und Analyse]. *Zeitschrift der Deutschen Gesellschaft für Geowissenschaften*, *162*(3), 235-250.

Bussolotto, M., Benedicto, A., Invernizzi, C., Micarelli, L., Plagnes, V. and Deiana, G., 2007. Deformation features within an active normal fault zone in carbonate rocks: The Gubbio fault (Central Apennines, Italy). *Journal of Structural Geology*, *29*(12), 2017-2037.

Bussolotto, M., Benedicto, A., Moen-Maurel, L. and Invernizzi, C., 2015. Fault deformation mechanisms and fault rocks in micritic limestones: Examples from Corinth rift normal faults. *Journal of Structural Geology*, *77*, 191-212.

Caine, J. S., Evans, J. P. and Forster, C. B. 1996. Fault zone architecture and permeability structure. *Geology*, **24**(11), 1025–1028.

Casolari, E., Negri, A., Picotti, V. and Bertotti, G., 2000. Neogene stratigraphy and sedimentology of the Gargano Promontory (southern Italy). *Eclogae Geologicae Helvetiae*, *93*(1), 7-24.

Catalano, R., D'argenio, B., Montanari, L., Morlotti, E. and Torelli, L., 1985. Marine geology of the NW Sicily offshore (Sardinia Channel) and its relationships with mainland structures. *Bollettino Della Societa Geologica Italiana*, *104*(2), 207-215.

Celico, F., Petrella, E. and Celico, P., 2006. Hydrogeological behaviour of some fault zones in a carbonate aquifer of Southern Italy: an experimentally based model. *Terra Nova*, *18*(5), pp.308-313.

Childs, C., Nicol, A., Walsh, J.J. and Watterson, J., 1996. Growth of vertically segmented normal faults. *Journal of Structural Geology*, *18*(12), pp.1389-1397.

Childs, C., Manzocchi, T., Walsh, J.J., Bonson, C.G., Nicol, A. and Schöpfer, M.P., 2009. A geometric model of fault zone and fault rock thickness variations. *Journal of Structural Geology*, *31*(2), pp.117-127.

Chilovi, C., de Feyter, A.J. and Pompucci, A., 2000. Wrench zone reactivation in the Adriatic Block; the example of the Mattinata fault system (SE Italy). *Bollettino della Società Geologica Italiana*, *119*(1), pp.3-8.

Cilona, A., Baud, P., Tondi, E., Agosta, F., Vinciguerra, S., Rustichelli, A. and Spiers, C.J., 2012. Deformation bands in porous carbonate grainstones: Field and laboratory observations. *Journal of Structural Geology*, *45*, 137-157.

Cilona, A., Solum, J.G., Lucca, A., Storti, F., Balsamo, F. and Taberner, C., 2019. Evolution of Pore Types and Petrophysical Properties of Fault Rocks in Low-Porosity Carbonates. *SEPM (Society for Sedimentary Geology)*, *18*(2), pp.94-107.

Cooke, A.P., Fisher, Q.J., Michie, E.A.H. and Yielding, G., 2018. Investigating the controls on fault rock distribution in normal faulted shallow burial limestones, Malta, and the implications for fluid flow. *Journal of Structural Geology*, *114*, 22-42.

Cooke, A.P., Fisher, Q.J., Michie, E.A.H. and Yielding, G., 2020. Permeability of carbonate fault rocks: a case study from Malta. *Petroleum Geoscience*, *26*(3), pp.418-433.

Cornée, J.J., Moissette, P., Joannin, S., Suc, J.P., Quillévéré, F., Krijgsman, W., Hilgen, F., Koskeridou, E., Münch, P., Lécuyer, C. and Desvignes, P., 2006. Tectonic and climatic controls on coastal sedimentation: the Late Pliocene–Middle Pleistocene of northeastern Rhodes, Greece. *Sedimentary Geology*, *187*(3-4), pp.159-181.

Corrado, S., Invernizzi, C. and Mazzoli, S., 2002. Tectonic burial and exhumation in a foreland fold and thrust belt: the Monte Alpi case history (Southern Apennines, Italy). *Geodinamica Acta*, *15*(3), 159-177.

Dart, C.J., Bosence, D.W.J. and McClay, K.R., 1993. Stratigraphy and structure of the Maltese graben system. *Journal of the Geological Society*, *150*(6), 1153-1166.

De Bresser, J.H.P. and Spiers, C.J., 1997. Strength characteristics of the r, f, and c slip systems in calcite. *Tectonophysics*, *272*(1), pp.1-23.

Delle Piane, C., Clennell, M.B., Keller, J.V., Giwelli, A. and Luzin, V., 2017. Carbonate hosted fault rocks: A review of structural and microstructural characteristic with implications for seismicity in the upper crust. *Journal of Structural Geology*, *103*, pp.17-36.

Droste, H. and Van Steenwinkel, M., 2004. Stratal geometries and patterns of platform carbonates: the Cretaceous of Oman.

Dunham, R.J., 1962. Classification of carbonate rocks according to depositional textures. In: Ham, W. E. (ed.), Classification of carbonate Rocks: American Association of Petroleum Geologists Memoir, p.108-121.

Evans, J.P., 1990. Thickness-displacement relationships for fault zones. *Journal of structural geology*, *12*(8), pp.1061-1065.

Færseth, R.B., 2006. Shale smear along large faults: continuity of smear and the fault seal capacity. *Journal of the Geological Society*, *163*(5), pp.741-751.

Ferraro, F., Grieco, D.S., Agosta, F. and Prosser, G., 2018. Space-time evolution of cataclasis in carbonate fault zones. *Journal of Structural Geology*, *110*, 45-64.

Ferraro, F., Agosta, F., Ukar, E., Grieco, D.S., Cavalcante, F., Belviso, C. and Prosser, G., 2019. Structural diagenesis of carbonate fault rocks exhumed from shallow crustal depths: An example from the central-southern Apennines, Italy. *Journal of Structural Geology, 122,* pp.58-80.

Ferraro, F., Agosta, F., Prasad, M., Vinciguerra, S., Violay, M. and Giorgioni, M., 2020. Pore space properties in carbonate fault rocks of peninsular Italy. *Journal of Structural Geology, 130,* 103913.

Ferrill, D.A. and Morris, A.P., 2008. Fault zone deformation controlled by carbonate mechanical stratigraphy, Balcones fault system, Texas. *AAPG bulletin*, *92*(3), 359-380.

Ferrill, D.A., Morris, A.P., McGinnis, R.N., Smart, K.J. and Ward, W.C., 2011. Fault zone deformation and displacement partitioning in mechanically layered carbonates: The Hidden Valley fault, central Texas. *Aapg Bulletin*, *95*(8), 1383-1397.

Fisher, Q. J. and Knipe, R. J. 1998. Fault sealing processes in siliciclastic sediments. *In: Jones, G., Fisher, Q. J. and Knipe, R. J. (eds) Faulting, Fault Sealing and Fluid Flow in Hydrocarbon Reservoirs. Geological Society, London, Special Publications*, **147**, 117–134.

Fisher, Q. and Knipe, R. 2001. The permeability of faults within siliciclastic petroleum reservoirs of the North Sea and Norwegian Continental Shelf. *Marine and Petroleum Geology*, **18**(2001), 1063–1081.

Flodin, E., Gerdes, M., Aydin, A. and Wiggins, W. 2005. Petrophysical properties and sealing capacity of fault rock, Aztec Sandstone, Nevada. *In: R. Sorkhabi and Y. Tsuji, (eds). Faults, Fluid Flow, and Petroleum Traps: AAPG Memoir*, **85**, 197–218.

Fondriest, M., Aretusini, S., Di Toro, G. and Smith, S.A., 2015. Fracturing and rock pulverization along an exhumed seismogenic fault zone in dolostones: The Foiana Fault Zone (Southern Alps, Italy). *Tectonophysics*, *654*, 56-74.

Fuchs, A., 1987. Conodont biostratigraphy of the Elbingerode reef complex, Harz Mountains. *Acta Geologica Polonica*, *37*(1-2), 33-50.

Giunta, G., Nigro, F. and Renda, P., 2000. Extensional tectonics during Maghrebides chain building since late Miocene: examples from Northern Sicily. In *Annales Societatis Geologorum Poloniae*, 70(1), 81-98.

Grobe, A., Urai, J.L., Littke, R. and Lünsdorf, N.K., 2016. Hydrocarbon generation and migration under a large overthrust: The carbonate platform under the Semail Ophiolite, Jebel Akhdar, Oman. *International Journal of Coal Geology*, *168*, pp.3-19.

Griggs, D.T., Turner, F.J. and Heard, H.C., 1960. Chapter 4: Deformation of rocks at 500° to 800° C. *Geol. Soc. Am. Mem*, *79*, pp.39-104.

Groshong Jr, R.H., 1988. Low-temperature deformation mechanisms and their interpretation. *Geological Society of America Bulletin*, *100*(9), 1329-1360.

Haines, T.J., Michie, E.A.H., Neilson, J.E. and Healy, D., 2016. Permeability evolution across carbonate hosted normal fault zones. *Marine and Petroleum Geology*, *72*, 62-82.

Hanken, N.M., Bromley, R.G. and Miller, J., 1996. Plio-Pleistocene sedimentation in coastal grabens, north-east Rhodes, Greece. *Geological Journal*, *31*(4), 393-418.

Holland, M., Urai, J.L., Muchez, P. and Willemse, E.J., 2009. Evolution of fractures in a highly dynamic thermal, hydraulic, and mechanical system–(I) Field observations in Mesozoic Carbonates, Jabal Shams, Oman Mountains. *GeoArabia*, *14*(1), 57-110.

Hugman III, R.H.H. and Friedman, M., 1979. Effects of texture and composition on mechanical behavior of experimentally deformed carbonate rocks. *AAPG Bulletin*, *63*(9), pp.1478-1489.

Jones, S., 1997. A technique for faster pulse-decay measurements in tight rocks. SPE Formation Evaluation, March, 19-25.

Kaminskaite, I., Fisher, Q.J. and Michie, E.A.H., 2019. Microstructure and petrophysical properties of deformation bands in high porosity carbonates. *Journal of Structural Geology*, *119*, 61-80.

Kaminskaite, I., Fisher, Q.J. and Michie, E.A.H., 2020. Faults in tight limestones and dolostones in San Vito lo Capo, Sicily, Italy: Internal architecture and petrophysical properties. *Journal of Structural Geology, 132,* 103970.

Kennedy, W.J. and Garrison, R.E., 1975. Morphology and genesis of nodular chalks and hardgrounds in the Upper Cretaceous of southern England. *Sedimentology*, *22*(3), 311-386.

Kim, Y.S., Peacock, D.C. and Sanderson, D.J., 2003. Fault damage zones. *Journal of structural geology*, *26*(3), 503-517.

Klinkenberg, L. J. 1941. The permeability of porous media to liquids and gases. *Drilling and Production Practice*, 200–213.

Knipe, R.J., 1992. Faulting processes and fault seal. In: Larsen, R. M., Brekke, H., Larsen, B. T. and Talle-Ras, E. (eds) *Structural and tectonic modelling and its application to petroleum geology.* Elsevier, Amsterdam, 1, pp. 325-342.

Kranz, R.L., 1983. Microcracks in rocks: a review. *Tectonophysics*, *100*(1-3), pp.449-480.

La Bruna, V., Agosta, F. and Prosser, G., 2017. New insights on the structural setting of the Monte Alpi area, Basilicata, Italy. *Italian Journal of Geosciences*, *136*(2), pp.220-237.

La Bruna, V., Agosta, F., Lamarche, J., Viseur, S. and Prosser, G., 2018. Fault growth mechanisms and scaling properties in foreland basin system: The case study of Monte Alpi, Southern Apennines, Italy. *Journal of Structural Geology*, *116*, 94-113.

Micarelli, L., Benedicto, A. and Wibberley, C.A.J., 2006. Structural evolution and permeability of normal fault zones in highly porous carbonate rocks. *Journal of Structural Geology*, *28*(7), pp.1214-1227.

Michie, E.A.H., Haines, T.J., Healy, D., Neilson, J.E., Timms, N.E. and Wibberley, C.A.J., 2014. Influence of carbonate facies on fault zone architecture. *Journal of Structural Geology*, *65*, 82-99.

Michie, E.A.H., 2015. Influence of host lithofacies on fault rock variation in carbonate fault zones: A case study from the Island of Malta. *Journal of Structural Geology*, *76*, 61-79.

Michie, E.A.H. and Haines, T.J., 2016. Variability and heterogeneity of the petrophysical properties of extensional carbonate fault rocks, Malta. *Petroleum Geoscience*, *22*(2), 136-152.

Michie, E.A.H., Yielding, G. and Fisher, Q.J., 2018. Predicting transmissibilities of carbonate-hosted fault zones. *Geological Society, London, Special Publications*, *459*(1), 121-137.

Molli, G., Cortecci, G., Vaselli, L., Ottria, G., Cortopassi, A., Dinelli, E., Mussi, M. and Barbieri, M., 2010. Fault zone structure and fluid–rock interaction of a high angle normal fault in Carrara marble (NW Tuscany, Italy). *Journal of Structural Geology*, *32*(9), 1334-1348.

Molli, G., White, J.C., Kennedy, L. and Taini, V., 2011. Low-temperature deformation of limestone, Isola Palmaria, northern Apennine, Italy–The role of primary textures, precursory veins and intracrystalline deformation in localization. *Journal of Structural Geology*, *33*(3), 255-270.

Peacock, D.C.P., 2001. The temporal relationship between joints and faults. *Journal of Structural Geology*, *23*(2-3), 329-341.

Pedley, H.M., House, M.R. and Waugh, B., 1976. The geology of Malta and Gozo. *Proceedings of the Geologists' Association*, *87*(3), 325-341.

Rath, A., Exner, U., Tschegg, C., Grasemann, B., Laner, R. and Draganits, E., 2011. Diagenetic control of deformation mechanisms in deformation bands in a carbonate grainstone. *AAPG bulletin*, *95*(8), 1369-1381.

Richard, P., Bazalgette, L. and Al-Kindi, M., 2014. North Oman fault geometries in outcrops, analogues and subsurface. *Geological Society, London, Special Publications*, *392*(1), 447-460.

Rotevatn, A., Thorsheim, E., Bastesen, E., Fossmark, H.S., Torabi, A. and Sælen, G., 2016. Sequential growth of deformation bands in carbonate grainstones in the hangingwall of an active growth fault: Implications for deformation mechanisms in different tectonic regimes. *Journal of Structural Geology*, *90*, pp.27-47.

Rustichelli, A., Torrieri, S., Tondi, E., Laurita, S., Strauss, C., Agosta, F. and Balsamo, F., 2016. Fracture characteristics in Cretaceous platform and overlying ramp carbonates: An outcrop study from Maiella Mountain (central Italy). *Marine and Petroleum Geology*, *76*, 68-87.

Schmoker, J.W. and Halley, R.B., 1982. Carbonate porosity versus depth: a predictable relation for south Florida. *AAPG bulletin*, *66*(12), pp.2561-2570.

Schröckenfuchs, T., Bauer, H., Grasemann, B. and Decker, K., 2015. Rock pulverization and localization of a strike-slip fault zone in dolomite rocks (Salzach–Ennstal–Mariazell–Puchberg fault, Austria). *Journal of Structural Geology*, *78*, 67-85.

Searle, M.P., 1985. Sequence of thrusting and origin of culminations in the northern and central Oman Mountains. *Journal of Structural Geology*, *7*(2), 129-143.

Shipton, Z.K. and Cowie, P.A., 2003. A conceptual model for the origin of fault damage zone structures in high-porosity sandstone. *Journal of Structural Geology*, *25*(3), pp.333-344.

Shipton, Z.K., Soden, A.M., Kirkpatrick, J.D., Bright, A.M. and Lunn, R.J., 2006. How thick is a fault? Fault displacement-thickness scaling revisited.

Solum, J.G. and Huisman, B.A.H., 2017. Toward the creation of models to predict static and dynamic fault-seal potential in carbonates. *Petroleum Geoscience*, *23*(1), pp.70-91.

Stead, J., 2018. The Impact of Burial History on the Permeability of Carbonate-Hosted Faults. MSc thesis. University of Leeds.ten Veen, J.H. and Kleinspehn, K.L., 2002. Geodynamics along an increasingly curved convergent plate margin: Late Miocene-Pleistocene Rhodes, Greece. *Tectonics*, *21*(3), 8-1.

ten Veen, J.H. and Kleinspehn, K.L., 2002. Geodynamics along an increasingly curved convergent plate margin: Late Miocene-Pleistocene Rhodes, Greece. *Tectonics*, *21*(3), pp.8-1.

Tondi, E., Antonellini, M., Aydin, A., Marchegiani, L. and Cello, G., 2006a. The role of deformation bands, stylolites and sheared stylolites in fault development in carbonate grainstones of Majella Mountain, Italy. *Journal of structural geology*, *28*(3), 376-391.

Tondi, E., Zampieri, D., Giunta, G., Renda, P., Alessandroni, M., Unti, M., Giorgianni, A. and Cello, G., 2006b. Active faults and inferred seismic sources in the San Vito lo Capo peninsula, northwestern Sicily, Italy. *Geological Society, London, Special Publications*, *262*(1), pp.365-377.

Tondi, E., 2007. Nucleation, development and petrophysical properties of faults in carbonate grainstones: evidence from the San Vito Lo Capo peninsula (Sicily, Italy). *Journal of Structural Geology*, *29*(4), 614-628.

Tondi, E., Rustichelli, A., Cilona, A., Balsamo, F., Storti, F., Napoli, G., Agosta, F., Renda, P. and Giorgioni, M., 2016. Hydraulic properties of fault zones in porous carbonates, examples from central and southern Italy. *Italian Journal of Geosciences*, *135*(1), 68-79.

Torabi, A. and Berg, S.S., 2011. Scaling of fault attributes: A review. *Marine and Petroleum Geology*, *28*(8), pp.1444-1460.

Torabi, A., Johannessen, M.U. and Ellingsen, T.S.S., 2019. Fault core thickness: Insights from siliciclastic and carbonate rocks. *Geofluids*, *2019*.

Tropeano, M. and Sabato, L., 2000. Response of Plio-Pleistocene mixed bioclastic-lithoclastic temperate-water carbonate systems to forced regressions: the Calcarenite di Gravina Formation, Puglia, SE Italy. *Geological Society, London, Special Publications*, *172*(1), 217-243.

Turner, F.J., Griggs, D.T. and Heard, H., 1954. Experimental deformation of calcite crystals. *Geological Society of America Bulletin*, *65*(9), pp.883-934.

Vandeginste, V., John, C.M., van de Flierdt, T. and Cosgrove, J.W., 2013. Linking process, dimension, texture, and geochemistry in dolomite geobodies: A case study from Wadi Mistal (northern Oman) Linking Process, Dimension, Texture, and Geochemistry in Dolomite Geobodies. *AAPG bulletin*, *97*(7), 1181-1207.

Van Dijk, J.P., Bello, M., Toscano, C., Bersani, A. and Nardon, S., 2000. Tectonic model and three-dimensional fracture network analysis of Monte Alpi (southern Apennines). *Tectonophysics*, *324*(4), 203-237.

Vandycke, S., 2002. Palaeostress records in Cretaceous formations in NW Europe: extensional and strike–slip events in relationships with Cretaceous–Tertiary inversion tectonics. *Tectonophysics*, *357*(1-4), 119-136.

Warren, J., 2000. Dolomite: occurrence, evolution and economically important associations. *Earth-Science Reviews*, *52*(1-3), pp.1-81.

Welch, M.J., Souque, C., Davies, R.K. and Knipe, R.J., 2015. Using mechanical models to investigate the controls on fracture geometry and distribution in chalk. *Geological Society, London, Special Publications*, *406*(1), 281-309.

Weller, H., 1991. Facies and development of the Devonian (Givetian/Frasnian) Elbingerode reef complex in the Harz area (Germany). *Facies*, *25*(1), 1.

Wibberley, C.A., Yielding, G. and Di Toro, G., 2008. Recent advances in the understanding of fault zone internal structure: a review. *Geological Society, London, Special Publications*, *299*(1), pp.5-33.

Yielding, G., Freeman, B. and Needham, D. 1997. Quantitative fault seal prediction. *AAPG Bulletin*, **6**(6), 897–917.

Yielding, G., Bretan, P. and Freeman, B. 2010. Fault seal calibration: a brief review. In: Jolley, S.J., Fisher, Q.J., Ainsworth, R.B., Vrolijk, P.K. and Delisle, S (eds) Reservoir Compartmentalization. Geological Society, London, Special Publications, 347, 243-255.

Yielding, G. 2015. Trapping of buoyant fluids in fault-bound structures. *Geological Society, London, Special Publications*, **421**(SP421-3).

Zambrano, M., Tondi, E., Mancini, L., Arzilli, F., Lanzafame, G., Materazzi, M. and Torrieri, S., 2017. 3D Pore-network quantitative analysis in deformed carbonate grainstones. *Marine and Petroleum Geology*, *82*, pp.251-264.

Zambrano, M., Tondi, E., Mancini, L., Lanzafame, G., Trias, F.X., Arzilli, F., Materazzi, M. and Torrieri, S., 2018. Fluid flow simulation and permeability computation in deformed porous carbonate grainstones. *Advances in water resources*, *115*, pp.95-111.

Figure Captions

Figure 1. Optical (taken under plane-polarised light (PPL)) and scanning electron microscope-backscatter electron microscopy (SEM-BSE) photomicrographs of carbonate host rocks with low how porosities from a variety of localities, illustrating the range of recrystallised textures. A: Elbingerode, Germany, recrystalised pack-grainstone; B: Sala Consilina, Italy, recrystallised mud-wackestone; C: Wadi Dayqah Dam, Oman, recrystallised oolitic grainstone; D: Wadi Al Nakhr, Oman, recrystallised wackestone; E: Wadi Al Bih, UAE, recrystallised pack-grainstone; F: San Vito Lo Capo, Sicily, Italy, recrystallised packstone.

Figure 2. Optical (taken under plane-polarised light (PPL)) and scanning electron microscope-backscatter electron microscopy (SEM-BSE) photomicrographs of carbonate host rocks with high host porosities from a variety of localities, illustrating the range of carbonate lithofacies; from wackestones, to packstones and grainstones. A: Favignana, Sicily, Italy, Grainstone; B: Pegwell Bay, UK, Chalk; C: Kallithea, Rhodes, Greece, Grainstones; D: Gozo, Malta, Packstone; E: Malta, wacke-packstone; F: Gozo, Malta, Algal-packstone.

Figure 3. Porosity and permeability plot of all measured fault rock samples.

Figure 4. Schematic plot showing the main fault rock microstructures observed with varying porosity and lithofacies type (how the texture is supported). Fault rocks originating from dispersed fracturing, leading to brecciation and cataclasis are observed at both low and high porosities, in those rock samples that are matrix-supported and supported by algae. Grain-scale fracturing leading to cataclasis occurs in clast-supported, highly porous samples. Note that low porosity samples are generally <10%, and high porosity sample are generally >10%.

Figure 5. A: Poro-perm plot of fault rock subdivided into lithofacies, based on the Dunham classification (Dunham 1962). B: Plot showing the inverse permeability contrast (fault rock permeability divided by host rock permeability) with varying lithofacies. Lithofacies is ordered by Dunham classification. All samples above 1 inverse permeability contrast show an increase in permeability ***relative*** to the host, and those below 1 inverse permeability contrast show a decrease in permeability ***relative*** to the host. Note no samples of mudstones have been collected.

Figure 6. Schematic diagram showing the main microstructures and respective permeabilities observed at different lithofacies juxtapositions. Square boxes are host samples, round boxes are fault rock samples. Blue and green: fault rock microstructures observed at self-juxtapositions of different lithofacies. Red: fault rock microstructures observed at juxtapositions with different lithofacies. This is an example from a packstone juxtaposed against an algal-packstone.

Figure 7. A: Graph showing the porosity and permeability of fault rocks that cut host rocks with different mineralogy. B: Graph showing porosity and permeability of fault rocks divided by current mineralogy.

Figure 8. Plots showing the porosity and permeability of host rock and fault rock samples, divided into low (<10%) and high (>10%) host porosities. Arithmetic averages of host porosity from each lithofacies per locality have been used to define faults that cut low (<10%) and high (>10%) host porosity lithofacies. Geometric averaging used for permeability values. A: All host poroperm points, and their respective average values, for low (<10%) host porosities. B: All host poroperm points, and their respective average values, for high (>10%) host porosities. C: Average host poroperm values and their respective fault rocks, for low average porosities (<10%). D: Average host poroperm values and their respective fault rocks, for high average porosities (>10%).

Figure 9. A and B: Graphs showing raw data for fault rock permeability with host porosity (A) and host permeability (B). C and D: Graphs showing weighted, geometrically averaged fault rock permeability with host porosity (C) and host permeability (D). Size of point correlates to the number of samples used for averaging, averaged per lithofacies, per locality. E and F: Graphs showing inverse permeability contract (fault rock permeability divided by the host rock permeability) with host porosity (E) and host permeability (F). The horizontal red line on E and F indicates no change in permeability from the host into the fault. The host porosity and permeability on each graph is the arithmetic and geometric average, respectively, per lithofacies, per locality. The correlation coefficient is shown for each trendline on each graph.

Figure 10. Top: Graph showing fault rock porosity and permeability split by kinematics (deformation bands, normal, oblique, strike-slip and thrust). Bottom: Microstructures of host and fault rocks from a strike-slip fault (left) and a normal fault (right).

Figure 11. A: Box and whisker plot showing fault rock permeability with binned displacements. Note that points binned at <1 m are deformation bands. B: Graph showing the inverse permeability contrast (fault rock permeability divided by host rock permeability) with displacement. Note that an arbitrary value of 0.01 m has been used for deformation bands, that show little to no displacement. C: Box and whisker plot showing fault rock permeability with displacement for an example of faults of varying displacement cutting a similar, low permeability, recrystallised host rock. Low displacement: *c.*10 m, high displacement: *c.*100 m. Box and whisker plots showing the minimum, maximum, interquartile and median values.

Figure 12. Optical photomicrographs showing host textures (A and C) and their respective fault rock textures (B and D). A: Plane polarised light photomicrograph of a recrystallised mudstone host sample from Sala Consilia, Italy. B: Plane polarised light photomicrograph of the associated fault rock from shallow burial depth (<1 km), showing brittle microstructures.

C: Plane polarised light photomicrograph of a recrystallised mud-wackestone host sample from Wadi Nakhr, Oman. D: Crossed-polarised light photomicrograph of the associated fault rock from high depth of burial (>6 km), showing ductile microstructures.

Figure 13. Graphs showing the raw fault rock permeability and geometrically averaged fault rock permeability per lithofacies, per locality, with maximum depth of burial (A) and depth at the time of faulting (B).

Table 1. Table summarising the key geological information of each main field locality.

Table 2. Single and multiple regression summary table using three main variable inputs: host porosity, host permeability and depth of burial, to assess which variable or combination of variables have the most significant control on fault rock permeability, where the higher the R^2 value and the lower the P-value, the higher the significance.

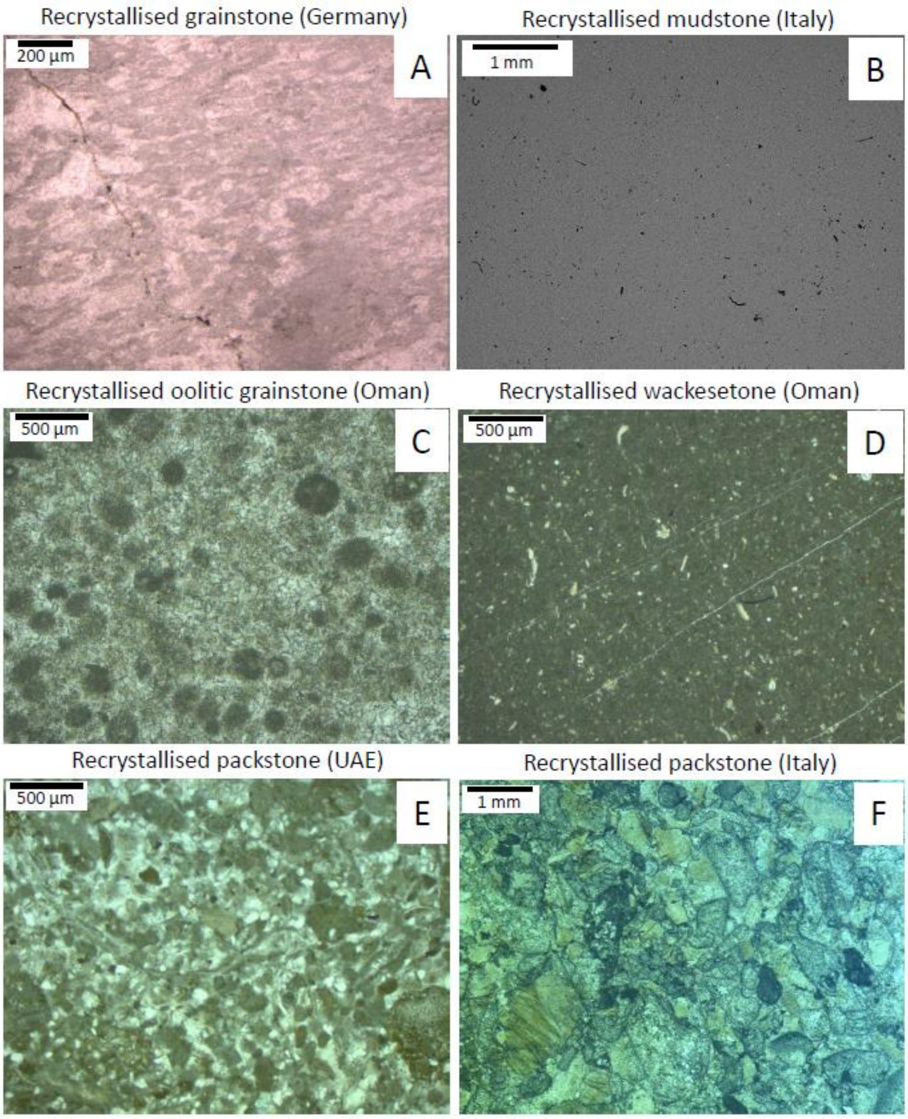
Recrystallised grainstone (Germany)
200 µm
A
Recrystallised mudstone (Italy)
1 mm
B
Recrystallised oolitic grainstone (Oman)
500 µm
C
Recrystallised wackesetone (Oman)
500 µm
D
Recrystallised packstone (UAE)
500 µm
E
Recrystallised packstone (Italy)
1 mm
F

Figure 1

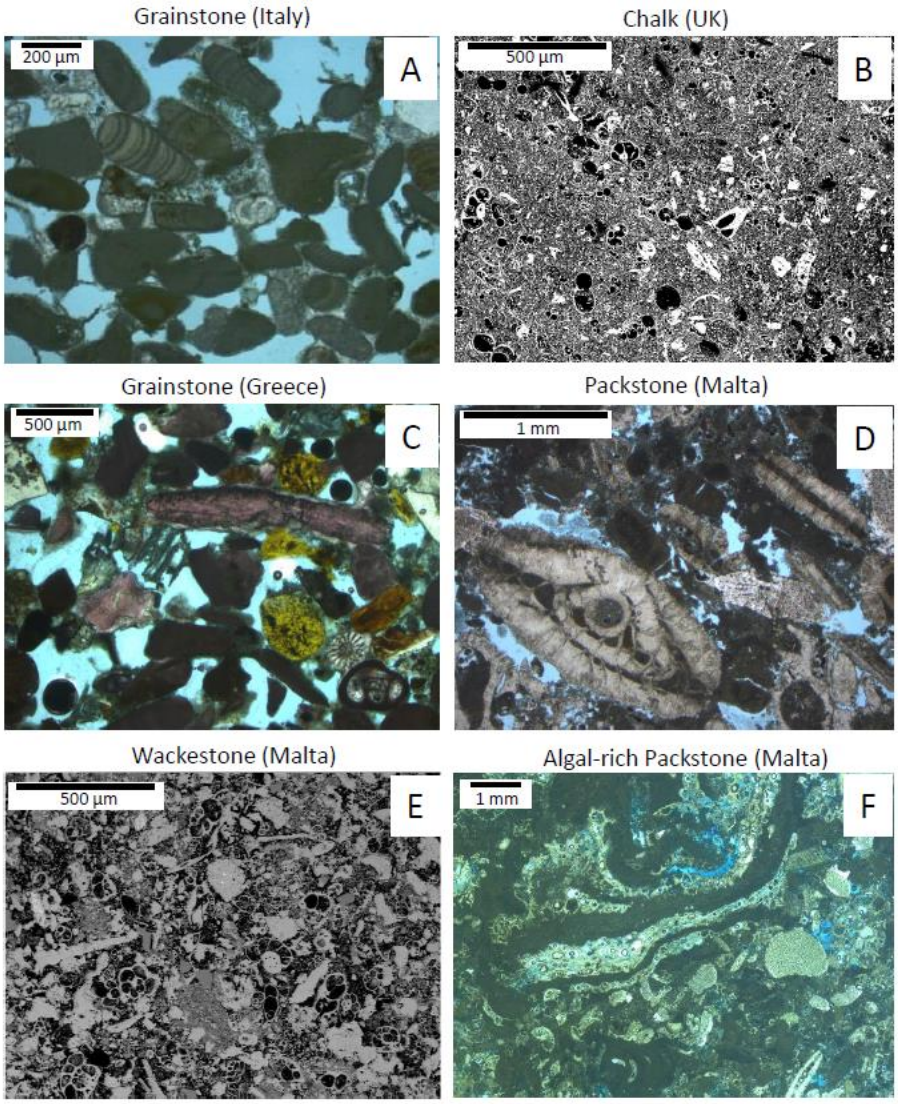
Grainstone (Italy)
200 µm
A
Chalk (UK)
500 µm
B
Grainstone (Greece)
500 µm
C
Packstone (Malta)
1 mm
D
Wackestone (Malta)
500 µm
E
Algal-rich Packstone (Malta)
1 mm
F

Figure 2

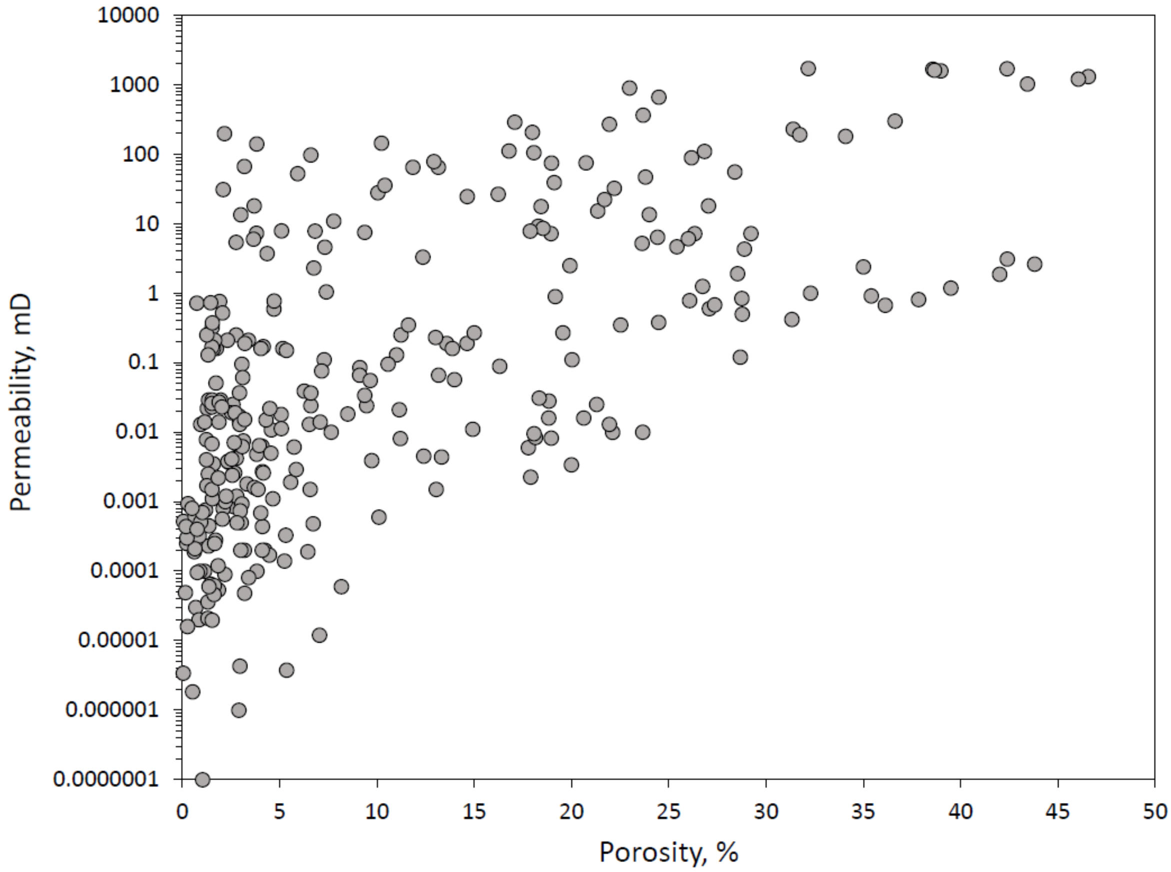
10000
1000
100
10
1
0.1
0.01
0.001
0.0001
0.00001
0.000001
0.0000001
Permeability, mD
0
5
10
15
20
25
30
35
40
45
50
Porosity, %

Figure 3

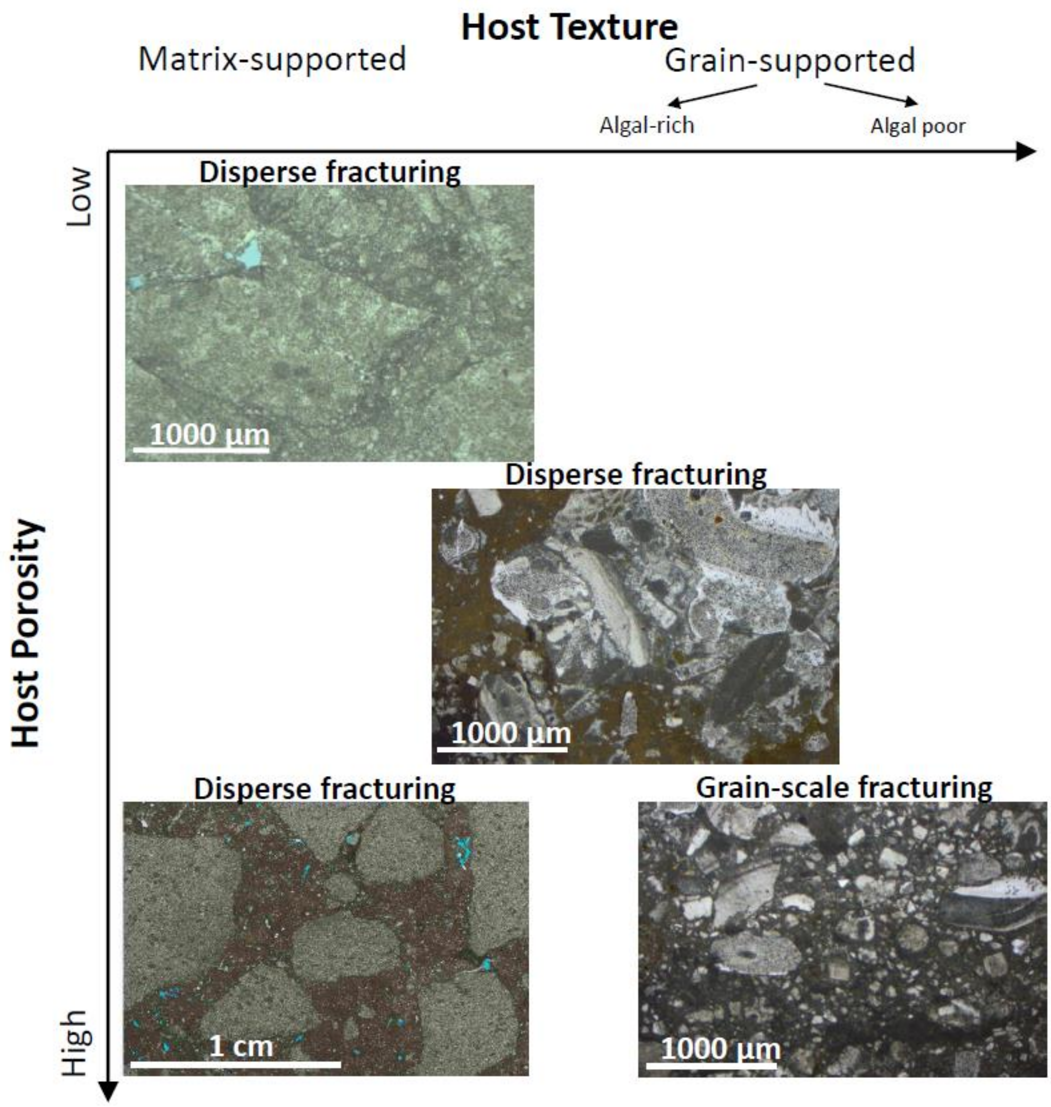

Host Texture
Matrix-supported
Grain-supported
Algal-rich
Algal poor
Low
High
Host Porosity
Disperse fracturing
1000 µm
Disperse fracturing
1000 µm
Disperse fracturing
1 cm
Grain-scale fracturing
1000 µm

Figure 4

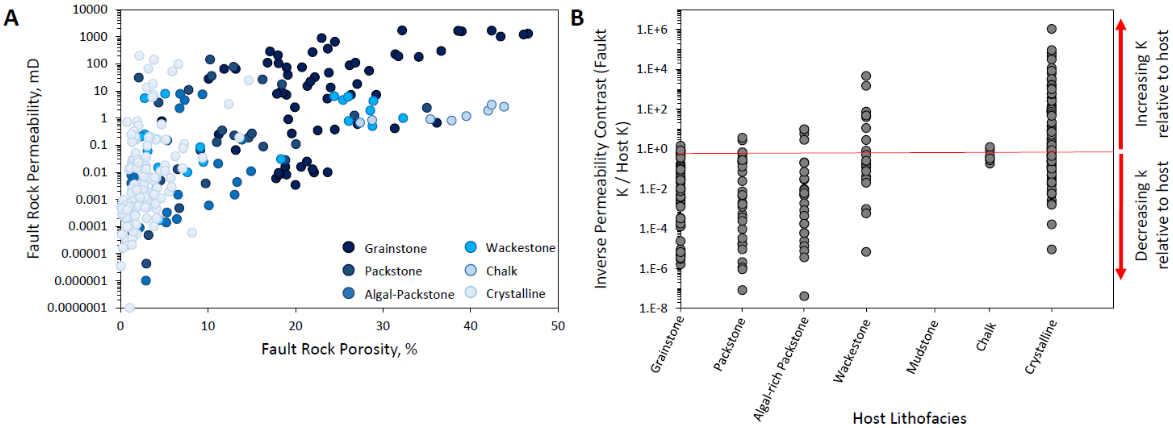
A
Fault Rock Permeability, mD
10000
1000
100
10
1
0.1
0.01
0.001
0.0001
0.00001
0.000001
0.0000001
0
10
20
30
40
50
Fault Rock Porosity, %
Grainstone
Packstone
Algal-Packstone
Wackestone
Chalk
Crystalline
B
Inverse Permeability Contrast (Faukt K / Host K)
1.E+6
1.E+4
1.E+2
1.E+0
1.E-2
1.E-4
1.E-6
1.E-8
Increasing K relative to host
Decreasing k relative to host
Grainstone
Packstone
Algal-rich Packstone
Wackestone
Mudstone
Chalk
Crystalline
Host Lithofacies

Figure 5

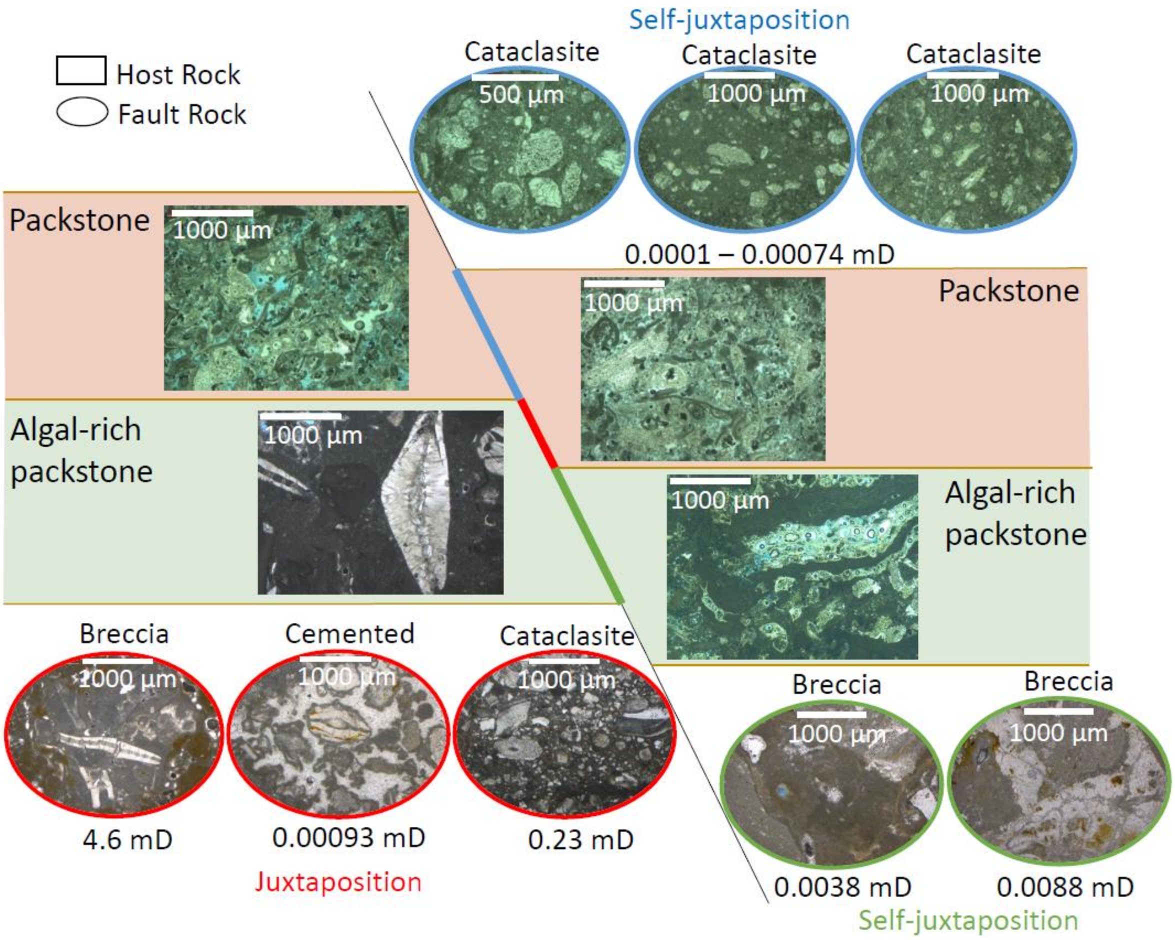
Self-juxtaposition
Cataclasite
Cataclasite
Cataclasite
Host Rock
Fault Rock
500 µm
1000 µm
1000 µm
0.0001 – 0.00074 mD
Packstone
1000 µm
1000 µm
Packstone
Algal-rich packstone
1000 µm
1000 µm
Algal-rich packstone
Breccia
Cemented
Cataclasite
1000 µm
1000 µm
1000 µm
Breccia
Breccia
1000 µm
1000 µm
4.6 mD
0.00093 mD
0.23 mD
Juxtaposition
0.0038 mD
0.0088 mD
Self-juxtaposition

Figure 6

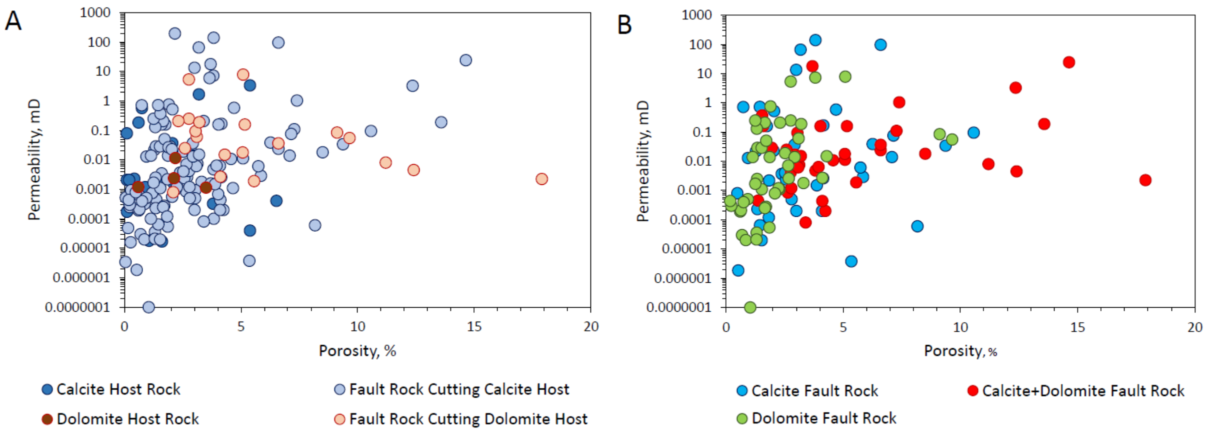
A
Permeability, mD
1000
100
10
1
0.1
0.01
0.001
0.0001
0.00001
0.000001
0.0000001
0
5
10
15
20
Porosity, %
Calcite Host Rock
Fault Rock Cutting Calcite Host
Dolomite Host Rock
Fault Rock Cutting Dolomite Host
B
Permeability, mD
Porosity, %
Calcite Fault Rock
Calcite+Dolomite Fault Rock
Dolomite Fault Rock

Figure 7

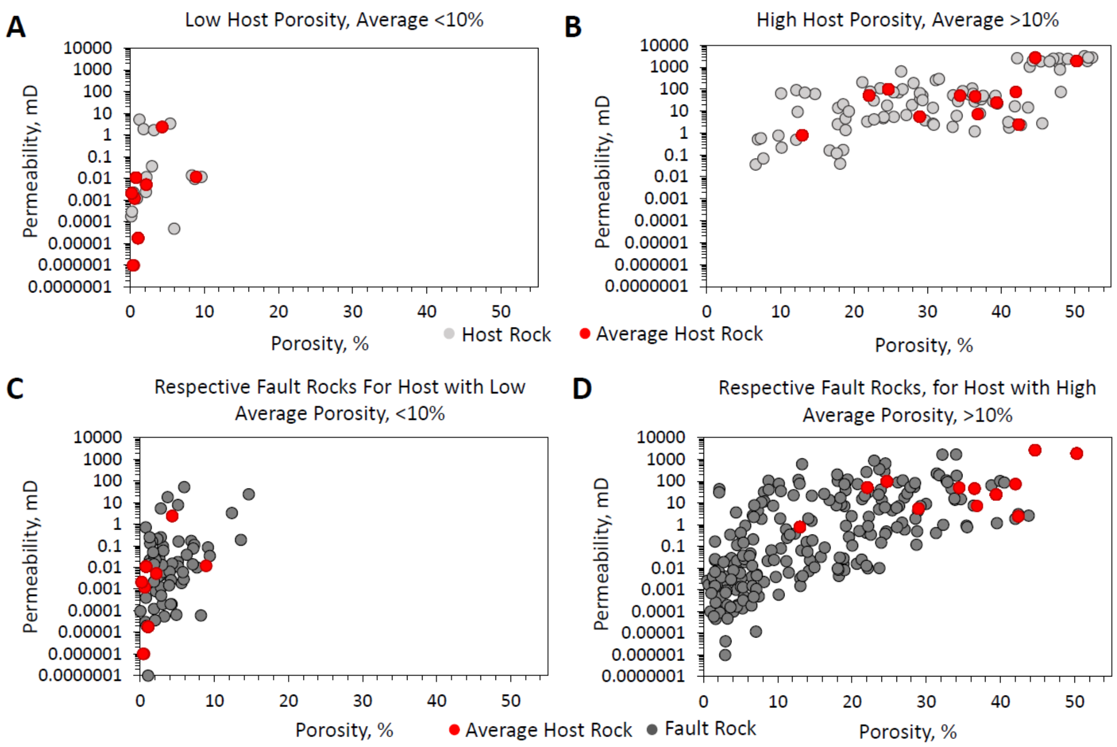
A
Low Host Porosity, Average <10%
Permeability, mD
Porosity, %
Host Rock
Average Host Rock
B
High Host Porosity, Average >10%
C
Respective Fault Rocks For Host with Low Average Porosity, <10%
D
Respective Fault Rocks, for Host with High Average Porosity, >10%
Fault Rock

Figure 8

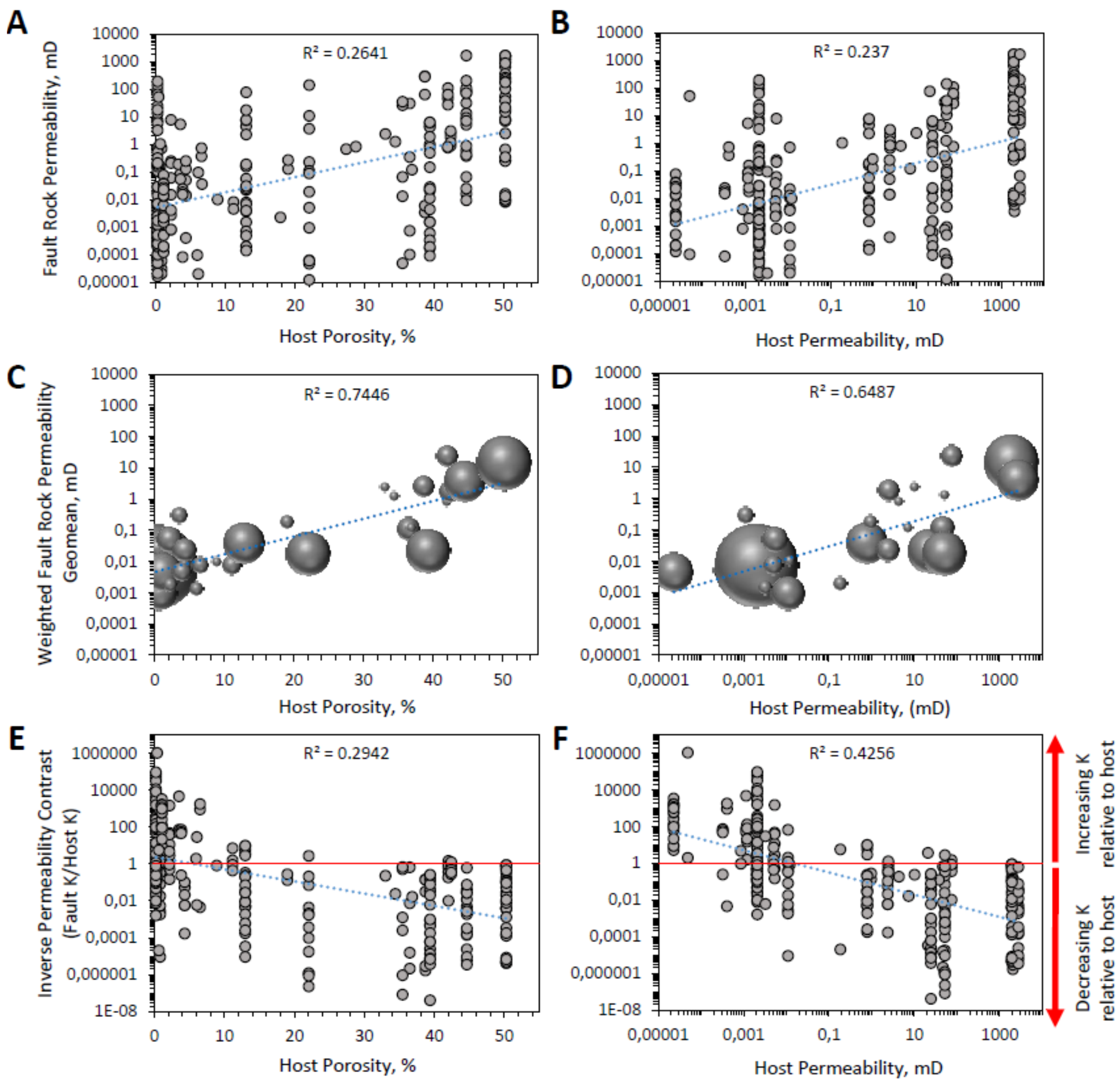

1159

1160 Figure 9

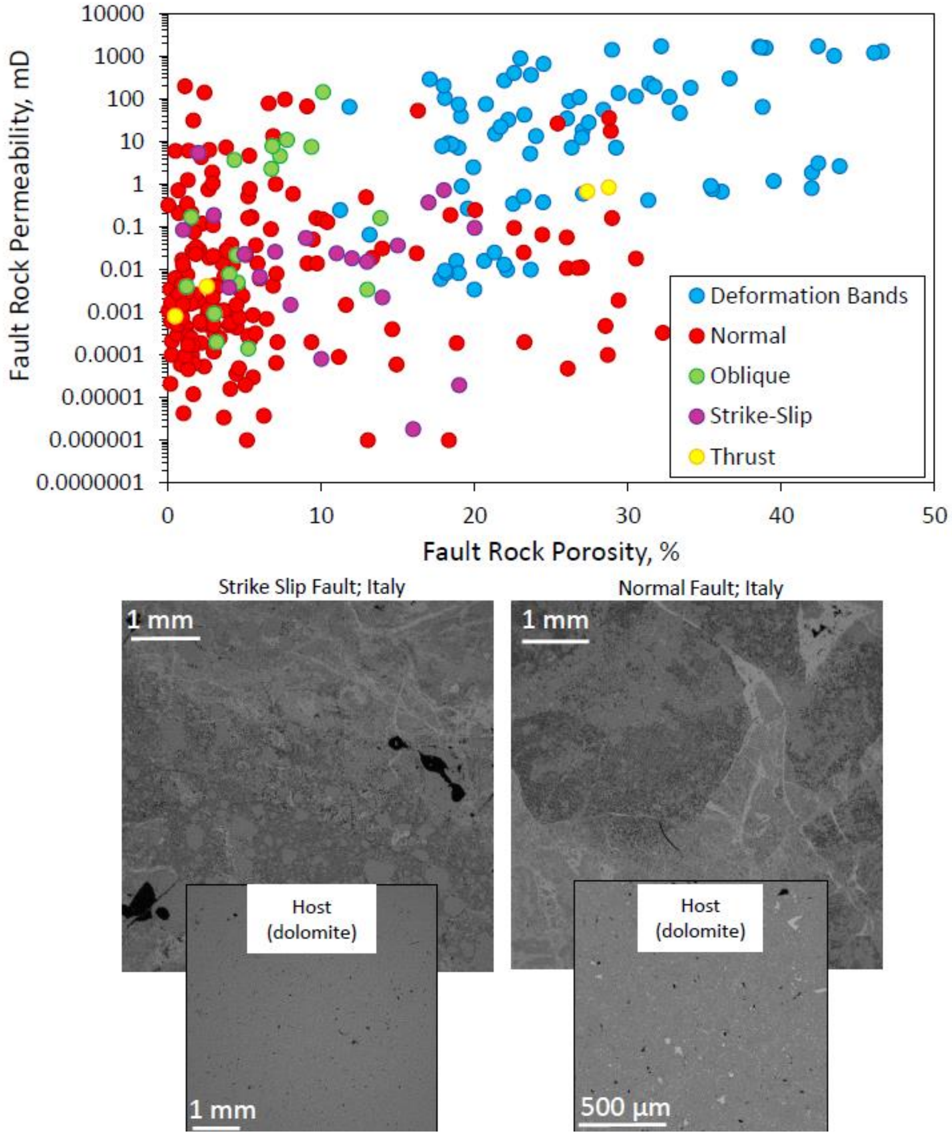

10000
1000
100
10
1
0.1
0.01
0.001
0.0001
0.00001
0.000001
0.0000001
Fault Rock Permeability, mD
0
10
20
30
40
50
Fault Rock Porosity, %
Deformation Bands
Normal
Oblique
Strike-Slip
Thrust
Strike Slip Fault; Italy
Normal Fault; Italy
1 mm
1 mm
Host (dolomite)
Host (dolomite)
1 mm
500 µm

Figure 10

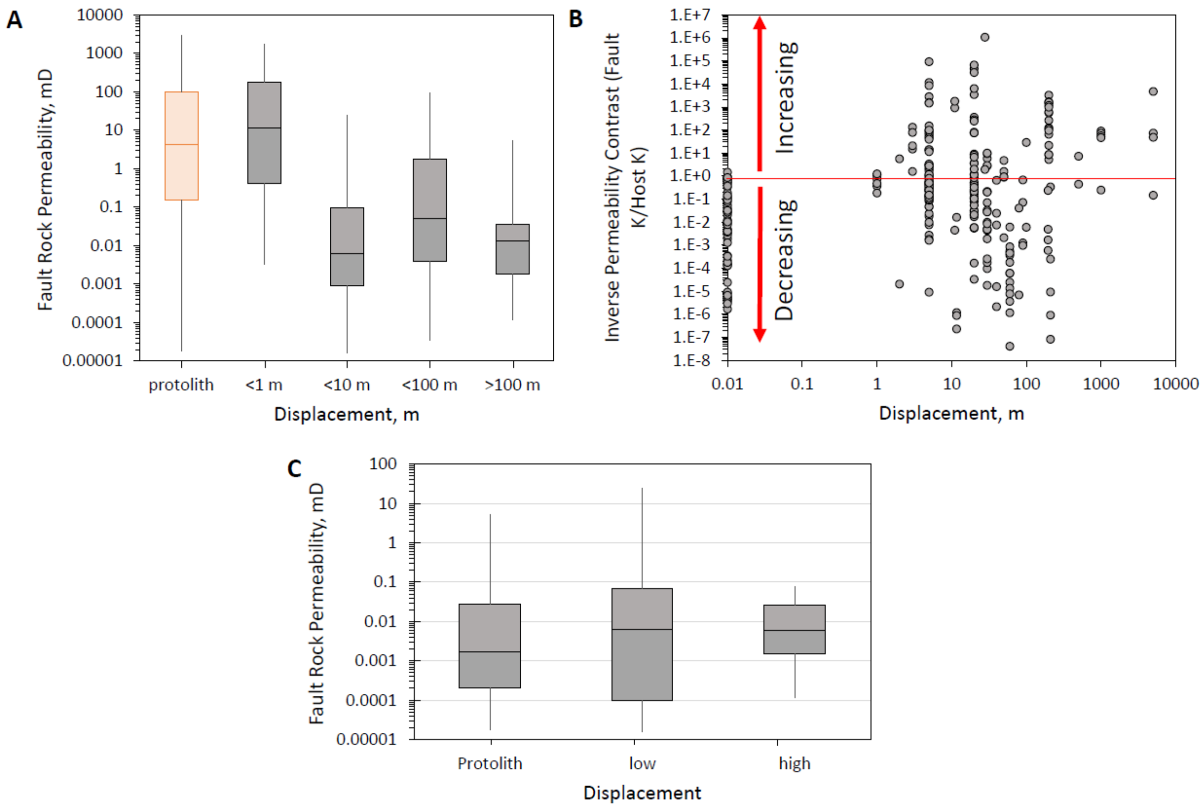

1163

1164 Figure 11

1165

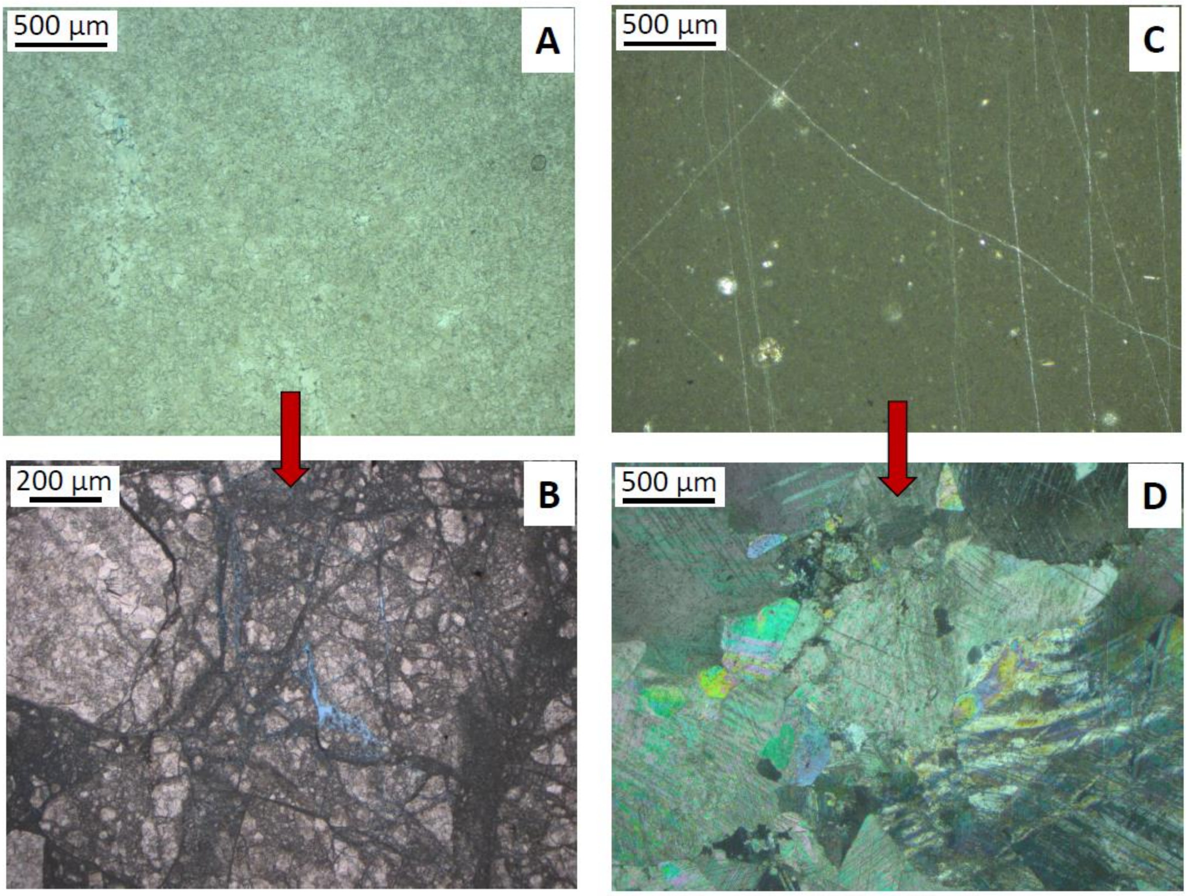

Figure 12

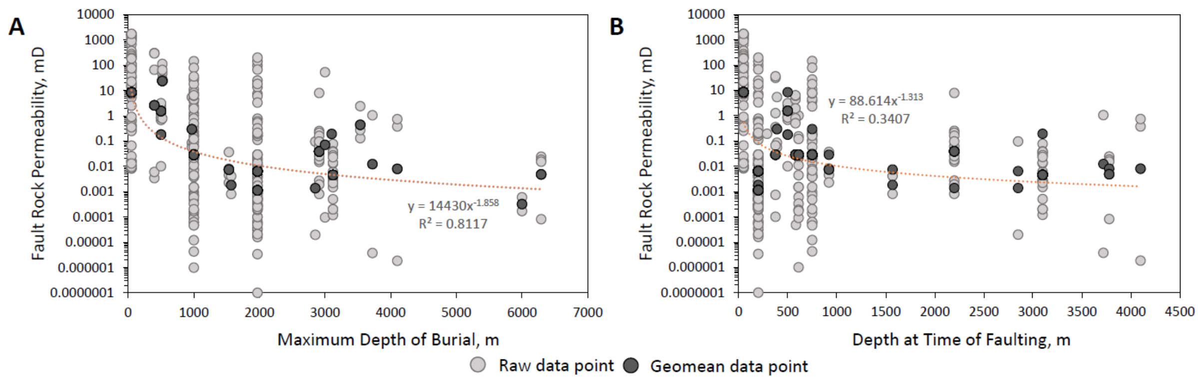

A
B
Fault Rock Permeability, mD
10000
1000
100
10
1
0.1
0.01
0.001
0.0001
0.00001
0.000001
0.0000001
0
1000
2000
3000
4000
5000
6000
7000
Maximum Depth of Burial, m
y = 14430x$^{-1.858}$
R^2 = 0.8117
500
1500
2500
3500
4500
Depth at Time of Faulting, m
y = 88.614x$^{-1.313}$
R^2 = 0.3407
Raw data point
Geomean data point

Figure 13

Locality	Lithofacies	Average Host Porosity, %	Average Host Permeability, mD	Displacement, m	Kinematics	Approximate Maximum Depth of Burial, m	Approximate Depth at time of faulting, m
Germany	Recrystallised	1.05	0.00002	100	Normal	3120	3100
Greece	Grainstone	43	900	<1	Def bands	520	Unknown
Italy; NW Sicily(a)	Grainstone	47.5	2000	<1	Def bands	50	50
Italy; NW Sicily(b)	Recrystallised	0.5	0.003	1-10s	Normal, Strike Slip	1970 - 3100	200 - 2200
Italy; SW Italy	Recrystallised	6	0.001	50-5000	Normal, Strike Slip	970 - 6290	390 - 3780
Italy; Gargano	Grainstone	38	2000	<1	Def bands	400	Unknown
Maltese Islands	Wackestone, Packstone, Algal Packstone	33 35 13	2 50 0.8	<1 - 210	Normal, Oblique, Strike Slip	300 - 1000	300 - 1000
Oman	Recrystallised	2	0.00001	28 - 50	Normal, Thrust	3000 - 6000	Several kilometres, but uncertain
UAE onshore	Recrystallised	3	0.004	2 - 100	Normal, Strike Slip, Thrust	1570 - 4100	1570 - 4100
UAE offshore	Wackestone, Packstone, Grainstone	25	5	<1 - 20	Def bands, Normal	2000 - 3500	Unknown
UK	Chalk	42	2.5	<1	Def bands	500	500

Table 1

Variable Input	Variable	R^2 Value	P-Value	Significance Summary
Host Porosity	Host Porosity	0.68	6.03E-08	Very High
Host Permeability	Host Permeability	0.55	1.094E-05	High
Host Porosity and Permeability	Host Porosity	0.66	0.0033	Medium
Host Porosity and Permeability	Host Permeability	0.66	0.68	Low
Host Porosity and Depth	Host Porosity	0.66	0.00015	Medium
Host Porosity and Depth	Depth of Burial	0.66	0.6	Low
Host Porosity, Permeability and Depth	Host Porosity	0.65	0.0018	Medium
Host Porosity, Permeability and Depth	Host Permeability	0.65	0.69	Low
Host Porosity, Permeability and Depth	Depth of Burial	0.65	0.6	Low

Table 2